

# Regional climate projections of mean and extreme climate for the southwest of Western Australia (1970–1999 compared to 2030–2059)

Julia Andrys<sup>1</sup> · Jatin Kala<sup>1,2</sup> · Thomas J. Lyons<sup>1</sup>

Received: 28 January 2016 / Accepted: 11 May 2016 / Published online: 21 May 2016  
© Springer-Verlag Berlin Heidelberg 2016

**Abstract** Projections of future climate change (1970–1999 compared to 2030–2059) for southwest Western Australia (SWWA) are analysed for a regional climate model (RCM) ensemble using the Weather Research and Forecasting Model with boundary conditions from three CMIP3 general circulation models (GCMs); CCSM3, CSIROmk3.5 and ECHAM5. We show that the RCM adds value to the GCM and we suggest that this is through improved representation of regional scale topography and enhanced land–atmosphere interactions. Our results show that the mean daytime temperature increase is larger than the nighttime increase, attributed to reduced soil moisture and hence increased surface sensible heat flux in the model, and there is statistically significant evidence that the variance of minimum temperatures will increase. Changes in summer rainfall are uncertain, with some models showing rainfall increases and others projecting reductions. All models show very large fluctuations in summer rainfall intensity which has important implications because of the increased risk of flash flooding and erosion of arable land. There is model consensus indicating a decline in winter rainfall and the spatial distribution of this rainfall decline is influenced by regional scale topography in two of the three simulations. Winter rainfall reduction is consistent with the historical trend of declining rainfall in SWWA, which has been attributed in previous research to a reduction in the number

of fronts passing over the region. The continuation of this trend is evident in all models by an increase in winter mean sea level pressure in SWWA, and a reduced number of winter front days. Winter rainfall does not show any marked variations in daily intensity.

**Keywords** Regional climate modelling · WRF · Western Australia

## 1 Introduction

High resolution projections of climate change are valuable for informing adaption planning and impact assessment studies. Industries as diverse as agriculture, forestry, conservation and urban planning can benefit from this information to help ensure their future viability. While general circulation models (GCMs) are currently the most authoritative resource on projected climate change, these models provide data at a resolution of 100–250 km that does not adequately represent finer scale influences on climate such as topography and land surface interactions (Mishra et al. 2012) nor do they allow for the adequate development of mesoscale weather systems (Salathé et al. 2010; Wehner et al. 2010; Donat et al. 2010). As a consequence, a knowledge gap exists between GCM output and the demand for high resolution climate data, particularly in those regions where local effects strongly influence the climate.

Regional climate models (RCMs) have been developed as one means to bridge this gap. By dynamically downscaling GCM data, RCMs can enhance the value of a GCM over limited areas by accounting for the influence of local topography and land use, therefore providing data at a resolution that can be useful for management strategies at a local scale. RCMs have been found to improve on the

✉ Julia Andrys  
j.andrys@murdoch.edu.au

<sup>1</sup> Environmental and Conservation Sciences, School of Veterinary and Life Sciences, Murdoch University Murdoch, Perth, WA 6150, Australia

<sup>2</sup> Australian Research Council Center of Excellence for Climate Systems Science, Sydney, NSW, Australia

representation of rainfall in GCMs (Feldmann et al. 2008; Song et al. 2008; Evans and McCabe 2013) as well as the distribution of extreme temperatures (Argüeso et al. 2012; Gao et al. 2012). However, RCMs introduce an additional level of uncertainty into future climate projections (Pielke and Wilby 2012), and as such the added value of using an RCM is not always guaranteed. Xue et al. (2014) examined the conditions that need to be met to establish whether a RCM adds value to the GCM being downscaled. These conditions include; establishing the merits of the model's domain set up, testing the sensitivity of its physics options, and finally evaluating historical RCM performance against observations, to determine how well the model can simulate the region's climatology and whether it can do this better than the GCM that is being downscaled. In addition to the dynamical downscaling approach employed by RCMs, statistical downscaling can also be applied to GCM data. These downscaling techniques are less computationally expensive compared to dynamical downscaling however they do not directly resolve regional dynamics and processes.

A further challenge when evaluating climate change scenarios lies in establishing whether changes are statistically significant. Because of the uncertainty associated with regional climate projections, some studies do not attempt to assign a statistical significance to their results (Gao et al. 2012; Salathé et al. 2010). One common approach has been to use a form of the Student's *t* test (Argüeso et al. 2012; Leibensperger et al. 2012) however this test assumes that climate variables are normally distributed which is not always the case, particularly when daily temperature distributions are considered (Perron and Sura 2013). Furthermore, the Student's *t* test only considers the significance of mean changes and does not provide a mechanism for testing the significance of other changes in the distribution, such as variance, skewness or kurtosis. Relative entropy ( $R_E$ ) has been used as a measure of the difference between observations and historical climate simulations (Tippett et al. 2004; Shukla et al. 2006; Andrys et al. 2015b), while Naveau et al. (2014) used  $R_E$  to detect historical trends in climate extremes. The  $R_E$  statistic, used in conjunction with a resampling technique following the method employed by Tippett et al. (2004), has scope to be used as a measure of the difference between future and historical climate variables that do not meet the necessary assumptions for the Student's *t* test because this method does not make any assumptions regarding the shape of the distribution.

This study focuses on the south west of Western Australia (SWWA), a globally recognised biodiversity hotspot (Malcolm et al. 2006), that has been found to be acutely at risk of negative impacts from climate change (Hughes 2003). Rising temperatures will put industries such as cropland farming and viticulture at risk (Webb et al. 2013)

while increased forest mortality events have been attributed to an increase in the diurnal temperature range (Evans and Lyons 2013). In terms of economic cost, changes to the region's hydrological regime present arguably the biggest risk because they threaten the yield of rain-fed cereal crops; the second largest export industry for the region (Varnas 2014). SWWA has already experienced reduced rainfall since the 1970s (Bates et al. 2008) which agricultural systems have been able to adapt to through a combination of advanced farming practices and because most of the rainfall decline has occurred in July and August, when rainfall exceeds cropping requirements (Turner and Asseng 2005). However, future changes in rainfall may impact the viability of agriculture in SWWA, especially in the marginal farming areas further inland. Hence, the demand for high resolution data on future climate projections is high. Hirsch et al. (2014) found that SWWA is a region of strong land-atmosphere coupling while Pitts and Lyons (1990) showed that model resolutions of 0.5 km were needed to fully represent the influence of topography on the regional meteorology. Because of these strong local influences, RCMs in the SWWA have the potential to add significant value to GCM projections.

This paper aims to explore future changes in mean and extreme climate for SWWA under a high emissions scenario using the Weather Research and Forecasting Model (WRF) Advanced Research Core. The utility of WRF as a RCM has been extensively evaluated for the region following the criteria recommended by Xue et al. (2014). Namely, Kala et al. (2015) conducted a sensitivity analysis of WRF to determine the most appropriate model physical parameterisations for SWWA. Andrys et al. (2015b) then used the best performing physical parameterisations from Kala et al. (2015) to carry out a 30-year climatology of SWWA using reanalysis boundary conditions from ERA-Interim (Dee et al. 2011) and showed that a 5 km domain provided a skillful representation of both mean and extreme climate variables. Following on from this work, Andrys et al. (2015a) evaluated the historical (1970–1999) performance of the model against observations with an ensemble of GCMs from the Coupled Model Intercomparison Project Phase 3 (CMIP3) and found that WRF was able to improve the representation of several climate variables, particularly rainfall intensity, when compared to the raw GCM output for three of the four GCMs that were evaluated. Based on this thorough evaluation of WRF for SWWA, and the skill shown by the model in reproducing historical climate when using GCMs as boundary conditions, we are confident that the RCM is indeed adding value to the GCMs in the study region. Therefore, we further extend on the work of Andrys et al. (2015a) here and compare near future (2030–2059) with historical (1970–1999) simulations to examine changes in temperature and precipitation and investigate

their drivers. In addition to examining daily temperature distributions and mean seasonal changes we also consider extreme climate indices and changes in the higher order statistical moments of daily climate variables. The  $R_E$  statistic is used for testing the significance of changes in daily variables.

## 2 Methods

### 2.1 Model description

The WRF RCM was set up following the configuration described by Andrys et al. (2015b). Regional climate simulations were carried out over 30 years between 1970–1999 and 2030–2059 from a single initialisation with a 2-month model spin-up using lateral boundary conditions from three CMIP3 GCMs. We note that CMIP5 (Taylor et al. 2012) now represents the current state of the art for GCMs however at the time these simulations were undertaken, the 6-hourly fields necessary to run WRF were not routinely available from the CMIP5 archive. The CMIP3 GCMs used include the Max Planck Institute ECHAM5 model (Roeckner 2003) (ECHAM), National Center for Atmospheric Research Community Climate System Model version 3 (CCSM) (Collins et al. 2006) and Commonwealth Scientific and Industrial Research Organisation Mark 3.5 (CSIRO) (Gordon et al. 2002). We use simulations following the SRES A2 emissions scenario (Nakićenović et al. 2000). GCMs used for boundary conditions were chosen based on the availability of 6-hourly data and with consideration of the GCM performance over Australia (Perkins et al. 2007). Andrys et al. (2015a) evaluated the historical performance of four CMIP3 GCMs which were down-scaled using WRF against observations. The three GCMs used in this study were found to represent the historical climate of SWWA skillfully, with the CCSM driven simulation providing the best results overall. A fourth simulation, which downscaled MIROC3.2 data has been excluded from this study because it was found by Andrys et al. (2015a) to demonstrate poor skill in representing the seasonal climate of SWWA.

The WRF model uses three nested domains (shown in Fig. 1) with a 50:10:5 km resolution. The choice of model physics follow the model configurations used in previous sensitivity studies and regional climate simulations in SWWA (Kala et al. 2015; Andrys et al. 2015a, b). Parameterisation options include the Single-Moment 5 class microphysics scheme (Hong et al. 2004), RRTM for long-wave radiation (Mlawer et al. 1997), Dudhia short-wave radiation (Dudhia 1989), Yonsei University planetary boundary layer scheme, the MM5 surface layer scheme (Grell et al. 2000) and Noah land surface model (Chen and Dudhia

2001). Convective parameterisation using Kain Fritsch (Kain 2004) is employed on the first and second domains only. The innermost 5 km domain explicitly resolves convection and has been found by Andrys et al. (2015b) to have the most accurate representation of rainfall, particularly in the cases of summer rainfall and rainfall around the Darling Scarp. Consequently, we focus our analysis on this domain. To help retain the large scale features from the lateral boundary conditions, the model uses spectral nudging. Nudging is applied in the outer domain only, above the PBL and for wavelengths exceeding 1000 km.

### 2.2 The southwest of Western Australia (SWWA)

The climate of the SWWA, illustrated in Fig. 2, is highly seasonal with cool wet winters and hot, dry summers. This seasonality is driven by the position of the subtropical high pressure belt (Gentilli 1971). The high pressure belt controls the passage of rain bearing cold fronts over the region in the winter and these frontal systems are the primary source of rain for much of the SWWA. Historical trends in SWWA indicate declining winter rainfall, attributed to a poleward shift of the subtropical ridge and hence a poleward shift of storm tracks (Frederiksen and Frederiksen 2007). A strong winter precipitation gradient is apparent between the region's comparatively wet coast and its dry interior.

Infrequent summer rainfall is caused by sporadic surface convection and large scale rain events which take place approximately every 3 to 5 years. Large scale rain events occur when the meridional coastal heat trough, a persistent summer feature, interact with tropical disturbances in the north of Western Australia, advecting moisture southwards (Wright 1974). Andrys et al. (2015a) found that while WRF was able to capture the magnitude of these summer rain events well over a 30 years climatology, the temporal distribution of this rainfall was replicated with less accuracy. WRF predicted rainfall events every 3–5 years however the timings of these events rarely correlated with observed events.

SWWA is an area of low relief, however local topography does influence the region's climatology, particularly coastal precipitation. The most notable topographical influence on climate is the Darling Scarp; an escarpment that produces a rapid change in elevation of approximately 300 m and runs parallel to the coast, 25 km inland (Fig. 1b). The escarpment results in a narrow band of elevated rainfall on its windward flank. Most of the agricultural production in SWWA takes place inland of the Darling Scarp and the growing season for these croplands is during the cooler months of May–October. During the growing season, the SWWA cereal crop is at risk from both frost and heat stress; research has found that screen temperatures below 2 °C and

above 34 °C can have a significant impact on grain yield (Zheng et al. 2012; Asseng et al. 2011). When Andrys et al. (2015b) evaluated WRF for SWWA using ERA-Interim reanalysis, they found a high negative rainfall bias in the extreme south west corner of the landmass which was attributed to the edge of the WRF domain being too close to the coastline. Because of the high bias in this region, we interpret results from this area with caution.

### 2.3 Evaluation criteria

We compare the 5 km resolution future climate simulations against the historical model simulations for the period 1970–1999 which were evaluated against observations by Andrys et al. (2015a) and found to represent the climatology of the region well, albeit with some systematic biases. In particular, daytime temperatures were found to have a cold bias of around 2 °C. To account for these biases, a clearer picture of projected change is possible by examining the change between future and historical simulations, as we assume that the same bias is inherent in both simulations. Because model output is not bias corrected, the projections we refer to in the Sects. 3 and 4 are not expectations of future climate in SWWA. Rather, they represent simulations of future climate for the purposes of model process understanding in the region.

Cold fronts are the major source of rainfall in SWWA and as such our evaluation needs to quantify the occurrence of fronts in the region. The thermal gradient recognition (TGR) method of Hope et al. (2014) for recognising fronts was found to detect SWWA cold fronts accurately and the technique was also employed by Andrys et al. (2015a) to compare simulated against observed front days. Here, we use TGR to compare the average number of winter front days between the historical and future climate periods for the 10 km domain. The approach detects baroclinicity using thermal gradients at the 850 hPa level. Following Andrys et al. (2015a) a front day is defined when the thermal gradient is  $>2.5 \text{ }^\circ\text{C } 100 \text{ km}^{-1}$  accompanied by daily domain averaged rainfall, for land based grid points only,  $>0.5 \text{ mm}$ .

We use indices developed by the World Meteorological Organisation working group, the Expert Team on Climate Change Detection and Indices (ETCCDI) (Persson et al. 2007) to explore changes in climate extremes between the historical and future simulations. With respect to temperature, we examine the mean annual diurnal temperature range (DTR), the hottest annual maximum temperature ( $\text{TX}_X$ ) and the coldest annual minimum temperature ( $\text{TN}_N$ ). During the SWWA growing season, cereal crops are at risk from heat stress above 34 °C (Asseng et al. 2011), consequently we measure the number of days in the growing season where temperatures exceed 34 °C using the summer days (SU) index. Frost is also a concern during the growing season and

Kala et al. (2009) has shown that screen temperatures below 2 °C are sufficient to result in foliage temperatures below 0 °C. Hence, we record the number of frost days (FD) when temperatures fall below 2 °C. The use of threshold-based indices allows for an exploration of climate change in the context of biologically important thresholds however, there are issues using this type of index when the model has large biases. These issues were demonstrated by Andrys et al. (2015a), where cold biases prevented one ensemble member from replicating threshold based indices. In this study we do not apply bias correction to model data, which limits the interpretation if these indices. However, Andrys et al. (2015a) also demonstrated that the three ensemble members we examine in this study had relatively small biases ( $<\pm 2 \text{ }^\circ\text{C}$ ) and were able to represent the historical SU and FD indices well. Hence we have confidence that these indices will be well represented by the non bias corrected data in this instance.

Rainfall intensity is measured by the simple precipitation intensity index (SDII);

$$SDII_j = \frac{\sum_{w=1}^W RR_{wj}}{W} \quad (1)$$

where  $RR_{wj}$  is the daily precipitation amount on days when rainfall is  $>1 \text{ mm}$  in period  $j$  and  $W$  is the number of days in  $j$  when rainfall is  $>1 \text{ mm}$ .

The total number of rain days (PRCPTOT) is a count of days where daily rainfall exceeds 1 mm. We also use the ETC-CDI metrics, maximum length of dry spell (CDD) and maximum length of wet spell (CWD). These indices measure the longest span of days where rainfall is  $<1 \text{ mm}$  for CDD and the longest span of days where rainfall is  $>1 \text{ mm}$  for CWD.

We calculate seasonal means of temperature and rainfall and for the precipitation indices SDII and PRCPTOT. Annual means are calculated for the remaining indices. The statistical significance ( $\alpha = 0.05$ ) of mean changes between the historical and future climate variables is quantified using the modified Student's  $t$  test following the methods described by Zwiers and von Storch (1995) to account for serial correlation.

Probability density functions (PDFs) are calculated for daily minimum and maximum temperatures.  $R_E$  between the historical and future distributions of these variables is then evaluated following Cover and Thomas (2012);

$$R_E(p||q) = \sum_{x \in X} p(x) \log \frac{p(x)}{q(x)} \quad (2)$$

where  $p(x)$  and  $q(x)$  are the historical and future simulation PDFs respectively. The statistical significance of the differences in the PDFs is calculated using a Monte Carlo resampling technique. Random samples, with a size of 10,000, are extracted from the historical distributions and the  $R_E$  of the sample with respect to the historical simulation is

calculated. This process is then repeated 1000 times and the sorted results provide the likelihood that the entropy of the future simulations exceeds the entropy of the historical simulation by chance. Changes in the future simulation are considered to be significant if they exceed the 95 % percentile of the sorted random relative entropy values. Sensitivity to the number of resamples taken was tested and it was found that increasing the number of repetitions above 1000 did not improve our results, hence we use this value for computational efficiency. This statistical method is applied in this instance because it is apparent that the distributions of daily temperatures do not follow a normal distribution. Furthermore, this method allows for an analysis of shifts in standard deviation and higher order statistical moments in the temperature distributions. This is achieved by subtracting the mean temperature from all data points and then applying the significance test to the standardised data.

Our conventions for illustrating an ensemble mean include displaying the mean only if all simulations agree on the direction of the change. Where simulations do not agree on the direction of the change the grid square is not shaded. Stippling is included on ensemble plots if all ensemble members agree on the direction of the change and that the change at that point is statistically significant.

### 3 Results

#### 3.1 Mean sea level pressure

We first examine the large scale changes by examining seasonal differences in mean sea level pressure (SLP) between

1970–1999 and 2030–2059 from the outer model domain (Fig. 1a) as shown in Fig. 3. Simulations show a consistent increase in SLP to the south of Western Australia during summer and winter with the SLP increase centered to the southwest in summer. Increases tend to correspond with areas of lower pressure (not shown). The simulation using ECHAM5 boundary conditions (W-ECH) shows the largest winter SLP increase in this region of up to 2 hPa while the CCSM and CSIRO driven simulations (W-CCS and W-CSI respectively) show a winter SLP increase in this region of approximately 1 hPa. Models demonstrate less consistency in SLP changes over the Australian landmass; winter SLP tends to show either no change or a small increase while summer SLP is decreasing in W-CCS, increasing in W-ECH and shows very little change in W-CSI. For all simulations the smallest changes to SLP are in autumn.

#### 3.2 Daily distribution of temperature

The PDFs for historical and future daily maximum temperatures for the 5 km domain are shown in Fig. 4a. It is apparent that distributions for future simulations are shifted to the right, indicating a greater likelihood of hotter temperatures. Additionally, the W-ECH and W-CSI simulations show that the frequency of the modal temperature is reduced, indicating that temperature spread has also increased. Summary statistics (Table 1) show that future simulations have an increased mean and standard deviation with reduced skewness and kurtosis. Figure 4b illustrates spatial differences in mean daily maximum temperatures, and stippling in this plot highlights that the distribution shift is statistically significant using the  $R_E$  test for significance described

**Table 1** Summary statistics ( $^{\circ}\text{C}$ ) for the distribution of daily maximum temperatures across the land based grid points of the 5 km domain for historical (1970–1999) and future (2030–2059)

	W-CCS Historical/future	W-ECH Historical/future	W-CSI Historical/future
Mean	22.23/23.75	20.72/21.88	23.22/24.93
Standard deviation	7.303/7.322	7.514/7.795	7.569/7.982
Skewness	0.466/0.436	0.517/0.462	0.439/0.404
Kurtosis	−0.651/−0.663	−0.502/−0.627	−0.741/−0.837

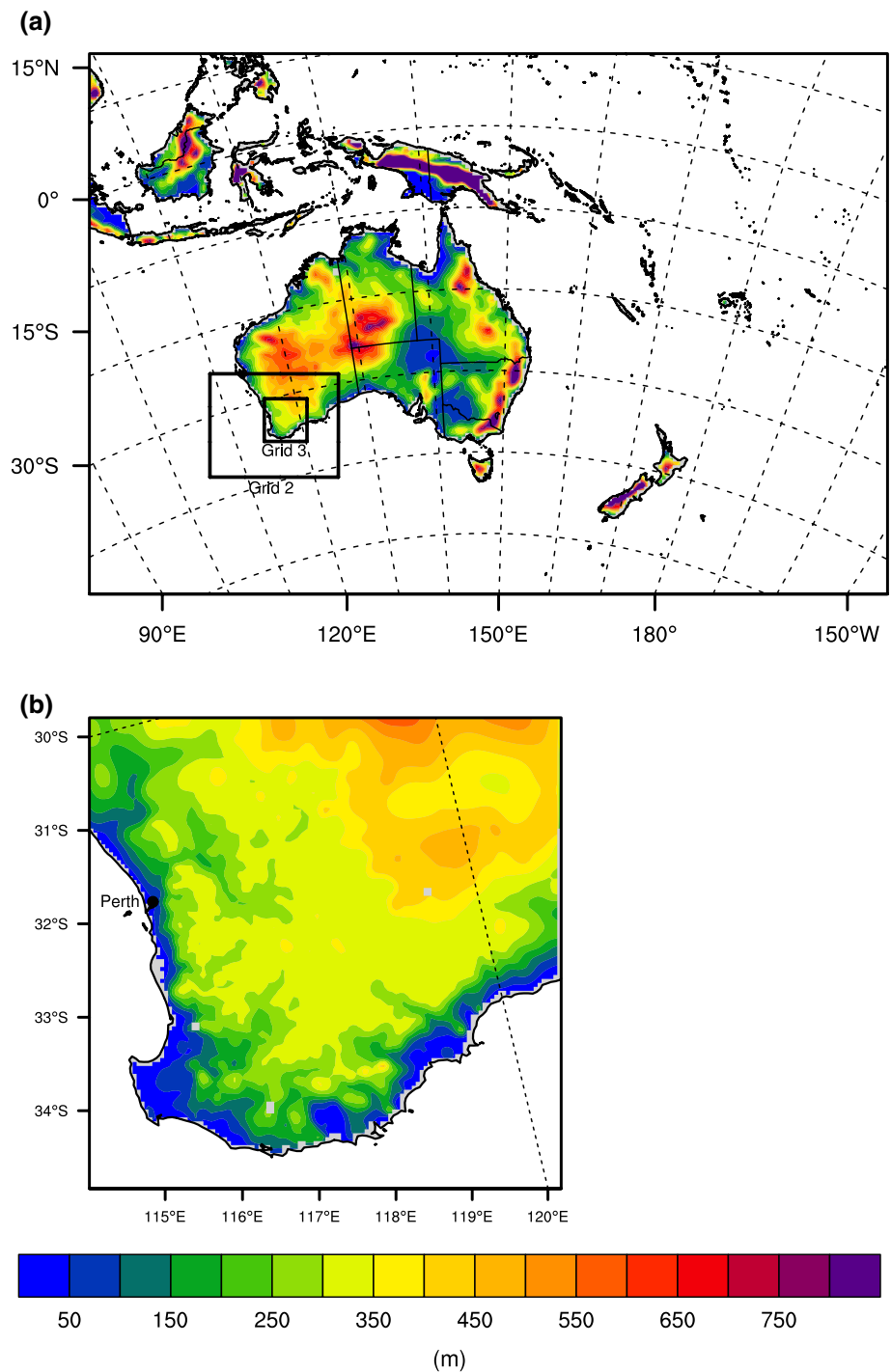
**Table 2** Same as in Table 1 but for minimum temperatures

	W-CCS Historical/future	W-ECH Historical/future	W-CSI Historical/future
Mean	10.49/11.80	10.44/11.34	12.05/13.42
Standard deviation	5.122/5.171	5.540/5.945	5.896/6.173
Skewness	0.259/0.266	0.344/0.331	0.261/0.269
Kurtosis	0.173/0.155	0.057/−0.138	−0.214/−0.243

**Table 3** Results from analysis of yearly summer rainfall showing the number of wet and dry summers for historical (1970–1999) and future (2030–2059)

	W-CCS	W-ECH	W-CSI
	Historical/future	Historical/future	Historical/future
Wet summer	2/4	15/17	10/9
Dry summer	28/26	15/13	20/21

**Fig. 1** Topographical map from Andrys et al. (2015b) of **a** the model outer domain showing the extent of nested grids 2 (10 km resolution) and 3 (5 km resolution) used for simulations and **b** the location of Perth and the topography of the Darling Scarp (area of rapidly increasing elevation from 0 to 300 m, extending from 31S to 34S, and between approximately 114.5E and 115.5E) within the 5 km domain



in Sect. 2.3. To determine whether changes in the standard deviation, skewness or kurtosis of the maximum temperature PDF are significant, we subtract the respective means from each distribution and apply the significance test to this standardised data. The results are illustrated in Fig. 4c, which shows differences in standard deviation and stippling to indicate where differences in the standardised distributions are statistically significant. It is apparent that the

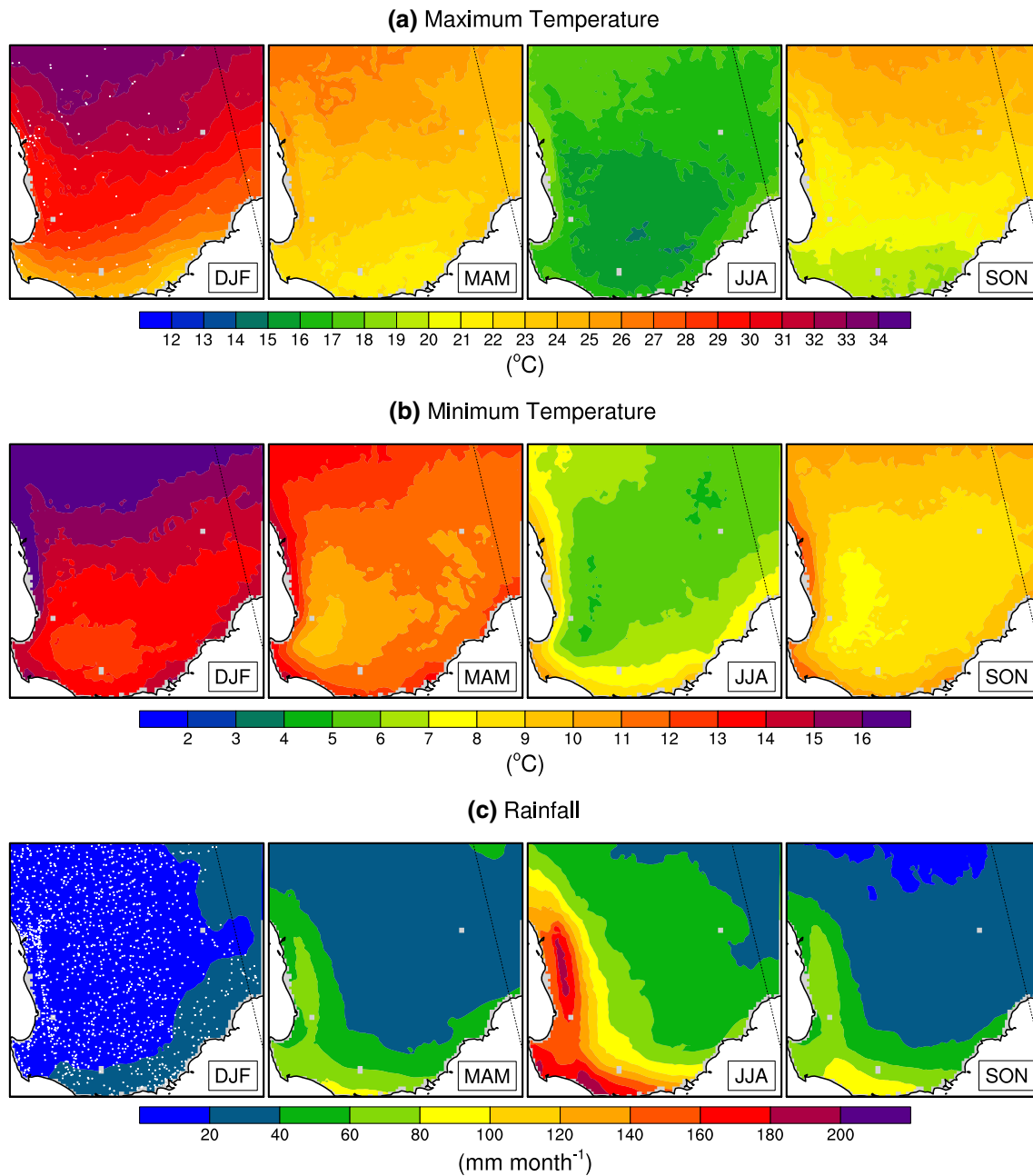


**Fig. 2** SWWA seasonal means of **a** maximum temperatures, **b** minimum temperatures and **c** rainfall between 1970–1999 for the 5 km domain using a gridded observational dataset from the Australian Bureau of Meteorology (Jones et al. 2009) from Andrys et al.

(2015b). The stations which have been used to generate the gridded data set are shown as *white dots* on the DJF plots in (a) for temperature and (c) for precipitation

standard deviation of maximum temperatures is expected to increase for both W-ECH and W-CSI however this change is not statistically significant. W-CCS shows only small differences in standard deviation and in the south east of the region this difference is negative and corresponds with statistically significant distribution differences. In addition, W-CCS shows areas where there are statistically significant differences between the standardised distributions with no

change to the standard deviation (areas where there is stippling but little to no change in the standard deviation). This suggests that these changes must be related to the higher order moments of skewness and/or kurtosis.

PDFs for historical and future daily minimum temperatures are shown in Fig. 5a and summary statistics for these distributions are shown in Table 2. The shift towards hotter future temperatures is apparent across all simulations

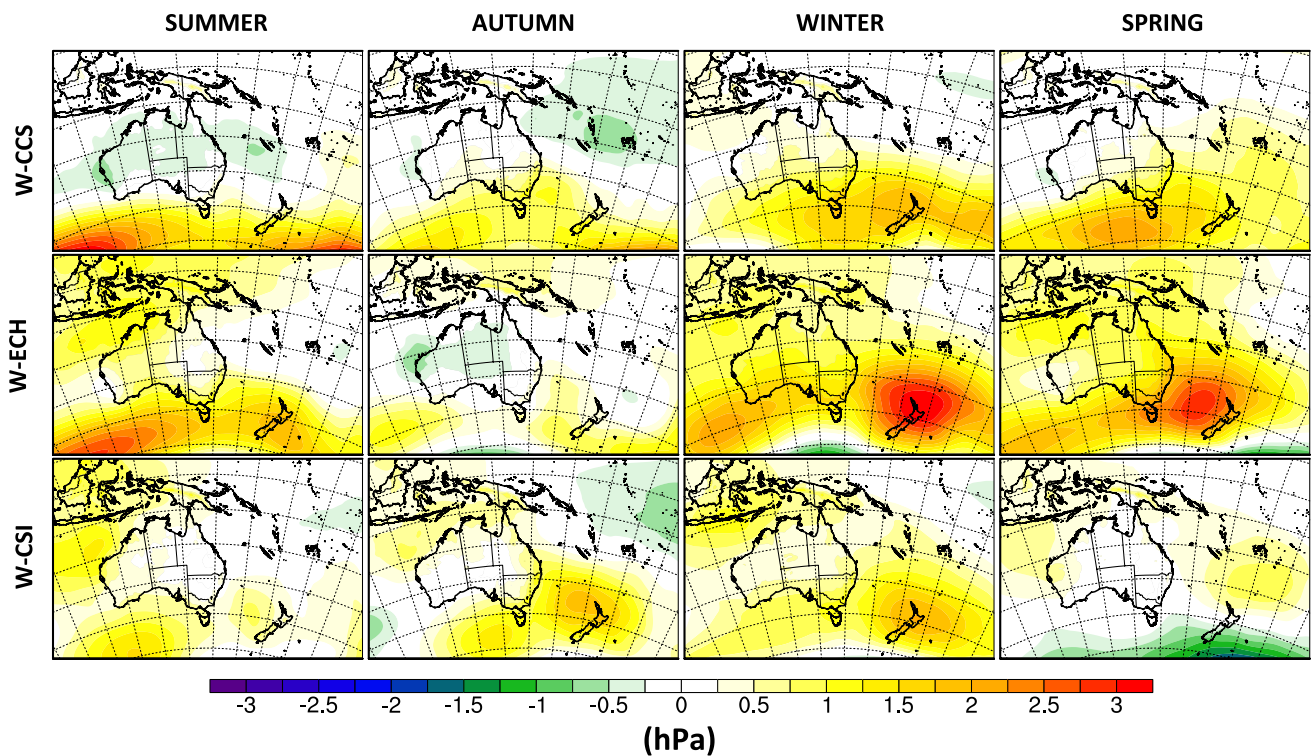


**Fig. 3** Seasonal mean sea level pressure difference between historical (1970–1999) and future (2030–2059) climate simulations for the WRF outer domain using CCSM3 (W-CCS), ECHAM5 (W-ECH) and CSIRO Mk 3 (W-CSI) lateral boundary conditions

and this is also shown by the increased daily temperature and the spatially consistent statistically significant changes shown in Fig. 5b. Figure 5c illustrates that simulated minimum temperature variance is expected to increase and there is model consensus on the statistical significance (using the  $R_E$  significance test) of differences between the standardised distributions in the north west of the region. Similar to maximum temperatures, we find that W-CCS is displaying areas with statistically significant differences between standardised distributions where there is little change in standard deviation indicating changes to skewness and/or kurtosis.

### 3.3 Seasonal changes in temperature and precipitation

The differences in mean seasonal temperatures between the GCMs and their corresponding RCMs are shown in Fig. 6. With the exception of W-CSI, the RCMs tend to underestimate temperature increases relative to the GCMs. The finer spatial resolution of the RCM also allows for a greater range of temperature change within the domain (up to  $1^\circ\text{C}$ ) as opposed to the GCM which in most cases finds the range of temperature change in the domain to be  $<0.5^\circ\text{C}$ . The increased spatial resolution of the RCM also shows greater warming on the west coast, particularly in the summer, which is not apparent in the GCMs.

Seasonal maximum temperature differences between the historical and future RCMs are shown in Fig. 7. Simulations show temperature increases in all seasons and these increases are statistically significant (using the modified Student's  $t$  test) across the domain with the exception of an area in the north east corner of the region in W-ECH. The simulations show that temperature increases will be the greatest along the west coast and in the north of the domain. W-CSI shows the largest increase, of up to  $3^\circ\text{C}$  during the summer while winter temperature increases tend to be no  $>2^\circ\text{C}$ . Seasonal minimum temperature differences are shown in Fig. 8. Similar to maximum temperatures, all minimum temperature changes are positive, by up to  $3^\circ\text{C}$  in W-CSI. However, overall increases are not as large as for maximum temperatures. Simulations agree that minimum temperature increases are significant for all seasons except for autumn and winter, when the W-ECH simulation does not show a significant increase over all areas of the landmass.

Differential changes between daytime and nighttime temperatures have been previously attributed to changes in cloud cover (Dai et al. 1999) and soil moisture (Fischer et al. 2007; Stéfanon et al. 2014). Hence, to attribute the spatial differences in these simulated temperature increases and the differential daytime and nighttime warming, we consider changes in seasonal cloud fraction and



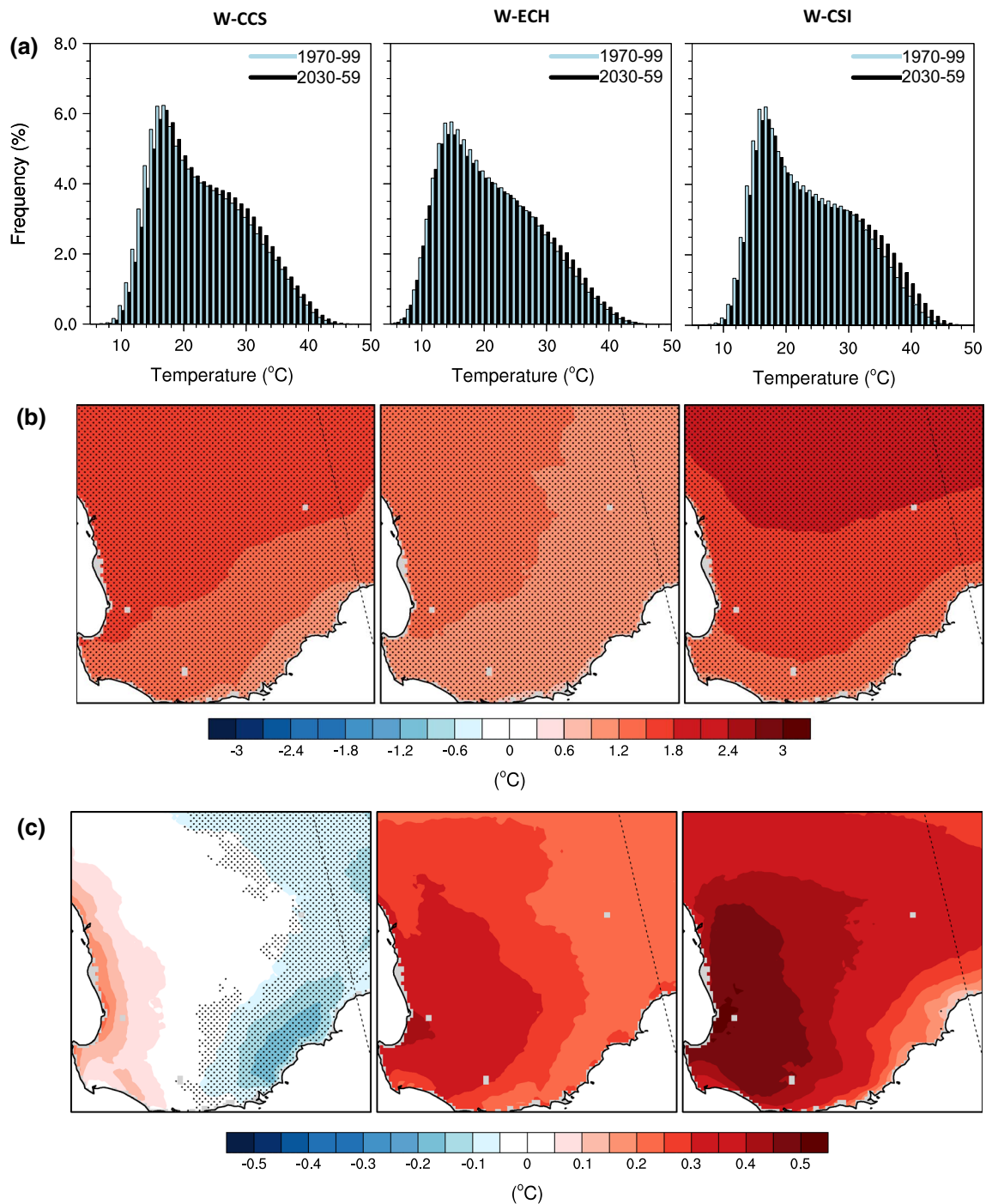


**Fig. 4** The distribution of historical (1970–1999) and future (2030–2059) daily maximum temperatures for the 5 km domain shown by **a** probability density functions (PDFs), **b** mean differences in daily maximum temperature with stippling displaying where differences in

the PDFs are significant at a 95 % confidence level and **c** differences in standard deviation with stippling highlighting where differences in standardised distributions (mean removed) are significant

soil moisture. Seasonal cloud fraction data is not shown because there are no marked differences in cloud cover (<0.3 %) found. Conversely, soil moisture (Fig. 9), which is predominantly driven by changes in rainfall, displays considerable differences. A decline in soil moisture is

consistent across all models in winter and spring however in the summer and autumn, W-CCS and W-ECH illustrate that areas in the east will have increased soil moisture. Soil moisture influences temperature by altering the partitioning of net radiation between sensible and latent heat flux, hence

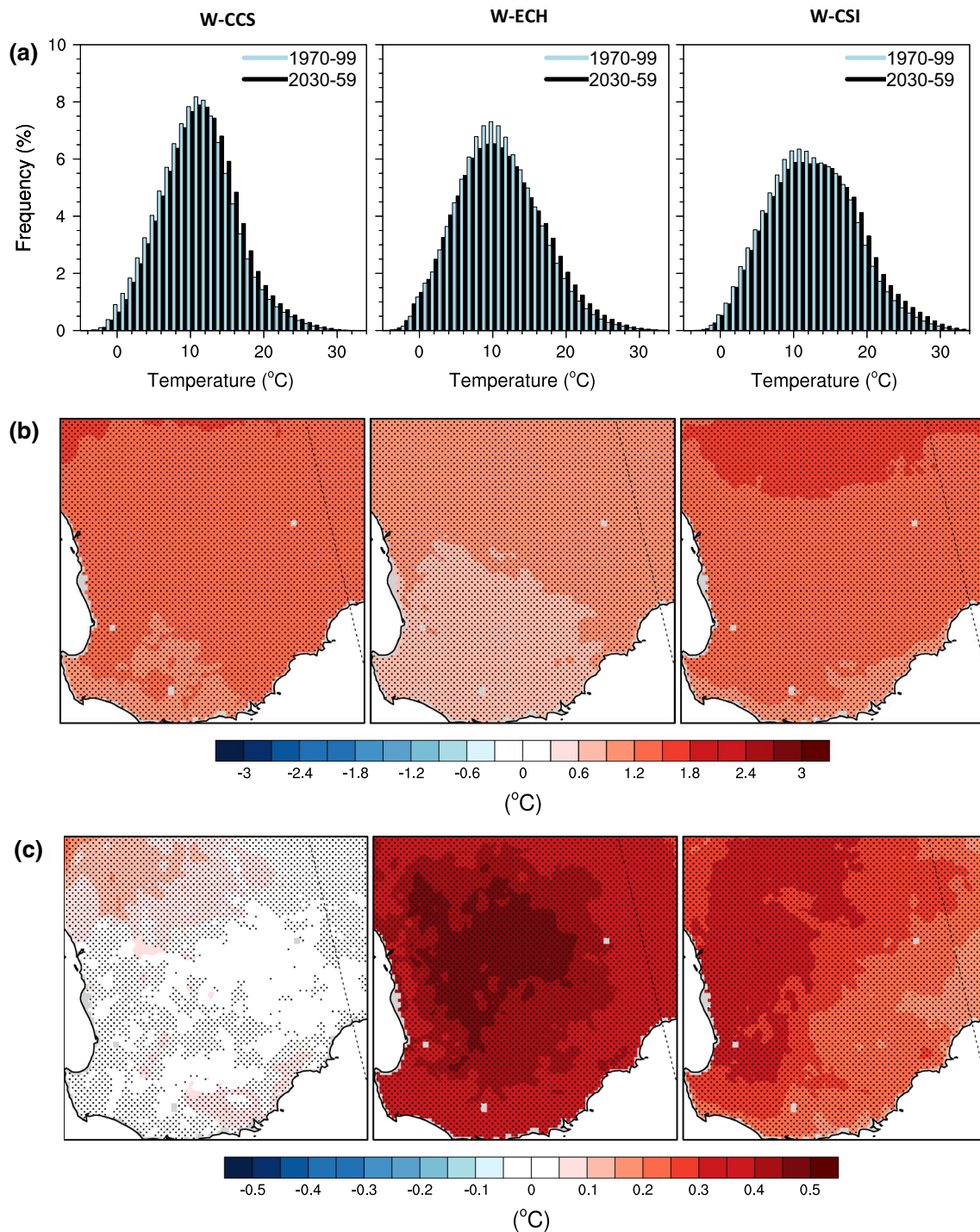


**Fig. 5** Same as in Fig. 4 but for minimum temperatures

we show seasonal surface sensible heat flux in Fig. 10 and it is apparent that areas of soil moisture deficit correspond with areas of increased sensible heat flux. For W-CCS and W-ECH, areas of increased surface sensible heat flux closely match areas with the highest daytime temperature increase, most notably in summer and spring.

Seasonal rainfall differences are shown in Fig. 11 for the GCMs and in Fig. 12 for the corresponding RCMs. GCMs and RCMs all show a decline in winter rainfall however there is less agreement between GCMs and RCMs in the other seasons. For example, both CCS and ECH show that summer precipitation will decline by up to 8 mm month<sup>-1</sup>

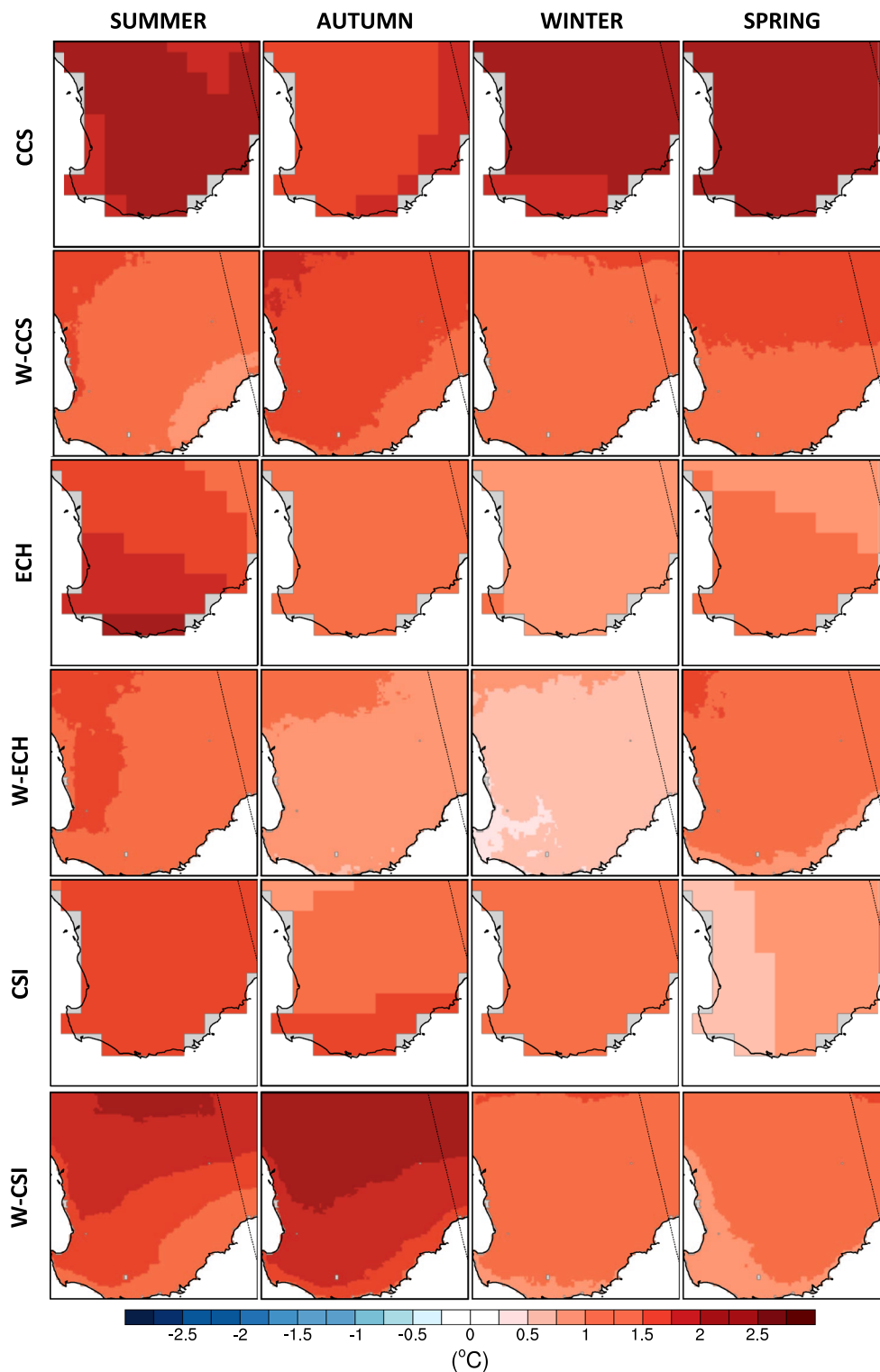


**Fig. 6** Mean seasonal temperature differences (1970–1999 to 2030–2059) for the GCMs CCSM (CCS), CSIRO (CSI), ECHAM5 (ECH) and the corresponding RCMs

while W-CCS and W-ECH show a small increase in rainfall. The improved spatial resolution of the RCM is better able to represent the influence of the Darling Scarp on

winter precipitation and the west to east precipitation gradient. It should be noted however that when the RCM model was evaluated by Andrys et al. (2015b), WRF displayed

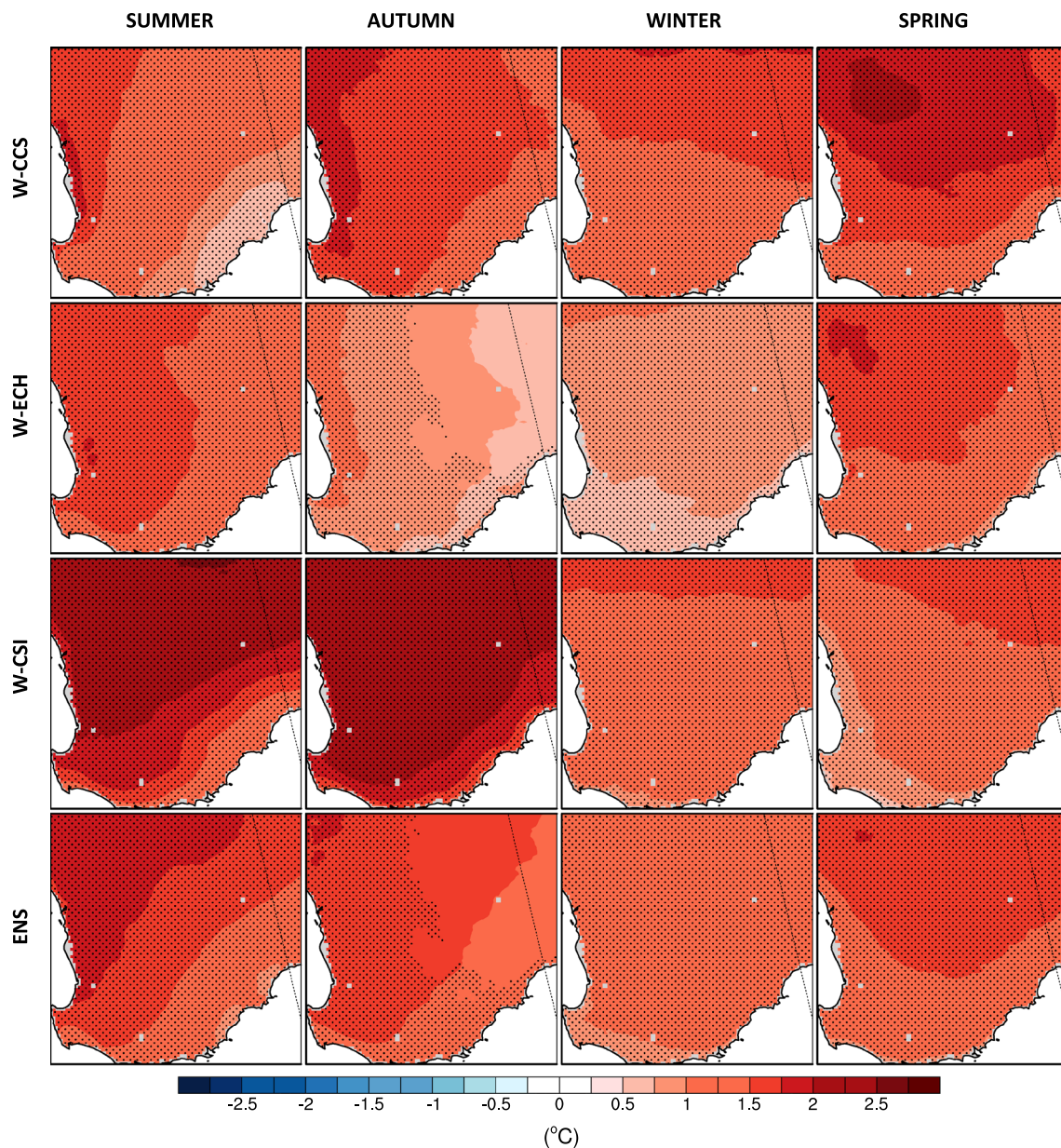


**Fig. 7** Seasonal mean maximum temperature differences between historical (1970–1999) and future (2030–2059) climate simulations. *Stippling* shows areas where there is a statistically significant difference in the distribution at a 95 % confidence interval

high negative rainfall biases in the far south west corner of the SWWA landmass. It is likely that results from this region have been impacted by this strong bias.

When the RCMs are compared with each other, simulations are not consistent on the direction of rainfall change. For example, the W-CCS and W-ECH simulations indicate that summer rainfall is likely to increase while W-CSI suggests that summer rainfall will decline. Models do agree that winter rainfall in the south west of the landmass will

decline however there is a large range with respect to the magnitude of this change and only W-ECH and W-CCS show the decline to be statistically significant. W-ECH shows that the reduction in rainfall in this region will exceed  $20 \text{ mm month}^{-1}$  while W-CSI suggests that rainfall decline will not exceed  $10 \text{ mm month}^{-1}$  and that some areas will receive more winter rainfall. The ENS plot highlights the model consensus on a decline in winter rainfall however it also illustrates the lack of model agreement on areas of

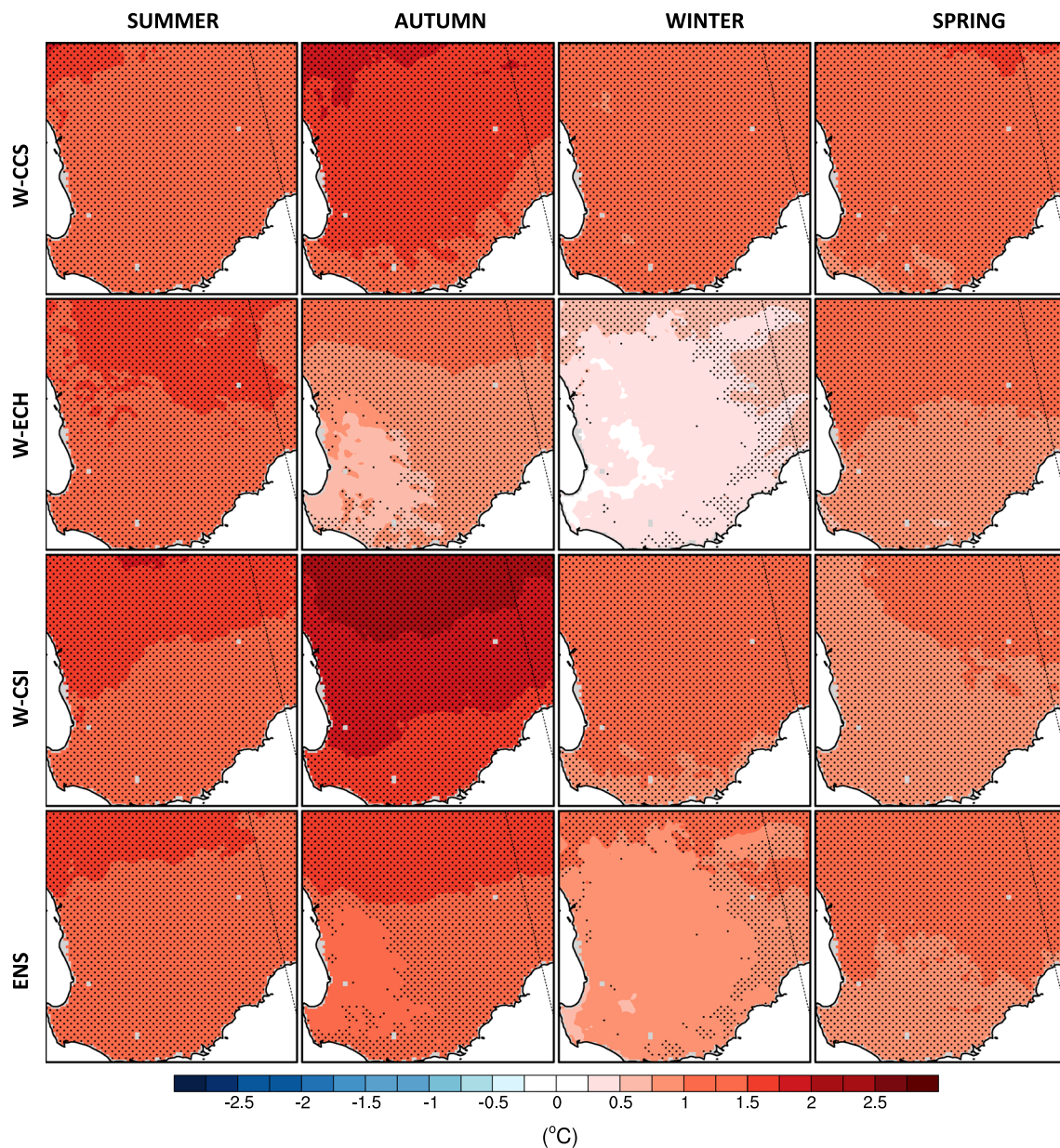


**Fig. 8** Same as in Fig. 7 but for minimum temperatures

significant rainfall change. Because winter rainfall is predominantly caused by cold fronts, we consider the number of winter front days present in the historical and future simulations as shown in Fig. 13. In all cases, there are fewer front days in the future simulation, however this difference is negligible in the W-CSI simulation (0.4 days a season).

To investigate why summer rainfall changes differ so markedly between simulations, we examine changes in the simulated number of large scale summer rainfall events. Observations show that SWWA experiences these rain events approximately once every 3–5 years and to evaluate how these events change in the

simulations, we follow the methodology of Andrys et al. (2015a) who define a wet summer as having at least one month where domain averaged rainfall exceeds 20 mm. These results are shown in Table 3. The incidence of large scale summer rainfall events doubles in the future W-CCS simulation, from a 1 in 10 years event to 1 in 5 years. However, there is no marked increase in the number of simulated rain events for W-ECH and W-CSI as the return value for these simulations remains relatively constant between the historical and future simulations at approximately 1 in 2 years and 1 in 3 years respectively.

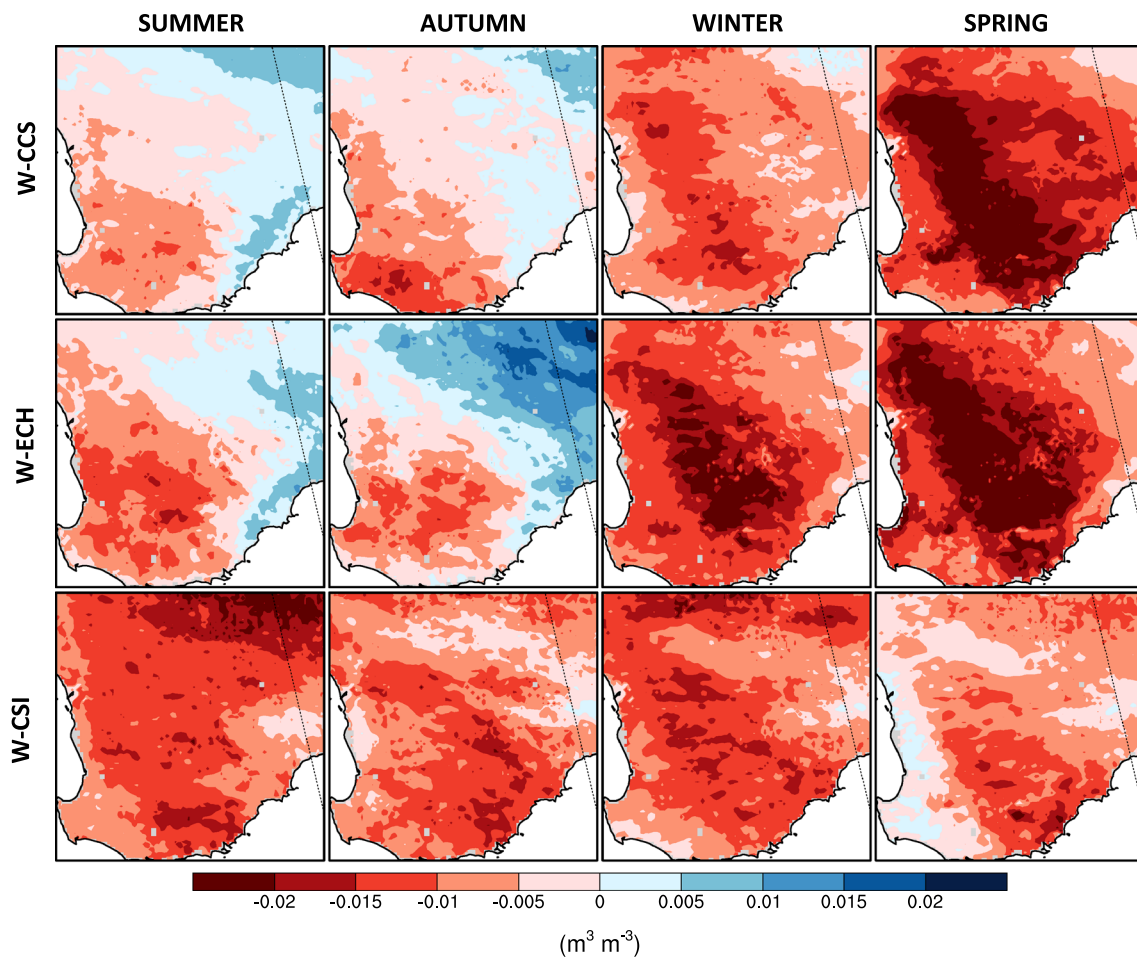


**Fig. 9** Seasonal mean surface soil moisture differences between historical (1970–1999) and future (2030–2059) climate simulations

### 3.4 Indices

Annually averaged differences in temperature indices are shown in Fig. 14. With the exception of the southern coast in the W-CCS simulation, all models agree that diurnal temperature range (DTR) will increase. Simulation DTR increases tend to be largest in the west and away from the moderating influences of the coast however none of the simulations show large areas of statistically significant changes when the modified Student's  $t$  test is applied.  $TN_N$ , a measure of the coldest nighttime temperature of the year, increases in the near future for W-CCS and W-CSI. W-ECH shows a small increase in most areas however in some cases W-ECH shows that the coldest nighttime temperatures will actually decline. Because of the low significance of changes to  $TN_N$  in W-ECH, ensemble agreement on a statistically significant change in  $TN_N$  is not spatially consistent. The hottest annual maximum temperature is measured by  $TX_X$ , and it is apparent that simulated future changes in  $TX_X$  are higher than changes to  $TN_N$ . W-CSI shows the highest increase in  $TX_X$ , of up to 3 °C on the south coast.

Simulations generally agree that this increase will exceed 1.2 °C throughout the domain. Ensemble changes in  $TX_X$  are also statistically significant over a greater portion of the domain than for  $TN_N$ .

Models agree that FD in the growing season is expected to decline for most of SWWA with the exception of the coastal region however Andrys et al. (2015b) demonstrated that under current climate, frost in the coastal region is already uncommon and hence unlikely to decline further. The reduction in frost is greatest in W-CCS, which shows up to 10 fewer FD every growing season. The ENS plot highlights the model consensus on a reduction in FD and also that models agree this decline is significant over the north of the region. An increase in growing season SU is expected in the north of SWWA for all models while the incidence of SU does not change in the south. Models are consistent on the spatial distribution of the increase in SU and also the magnitude of the increase, with the very north of the region expecting up to 3 more SU each growing season. This increase to the north of the region is statistically significant for all models in patches, which is highlighted by the ENS plot.

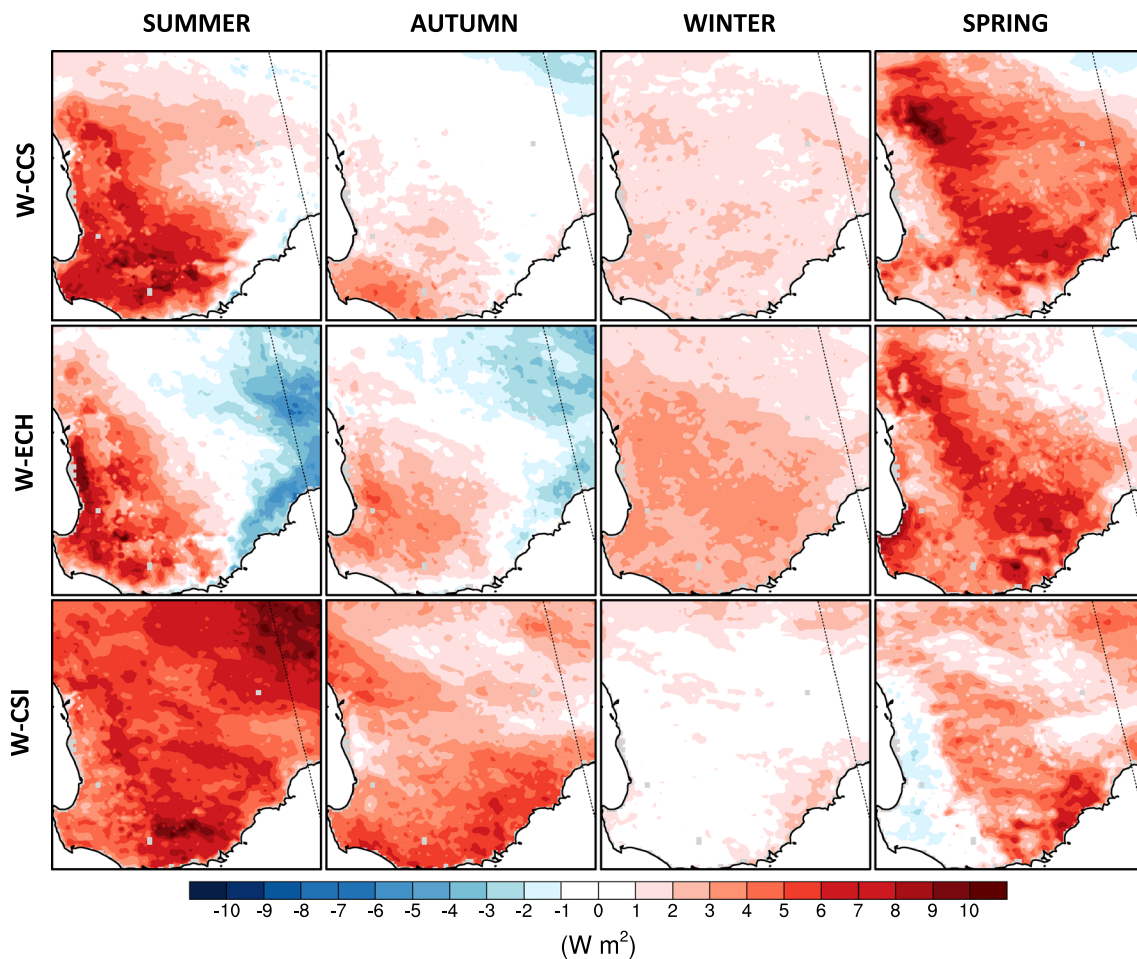


**Fig. 10** Same as in Fig. 9 but for surface sensible heat flux

Figure 15 shows changes in summer and winter rainfall SDII and PRCPTOT and annual CWD and CDD. Simulations show small and generally insignificant changes in winter SDII and models do not agree on the direction of these changes. Simulations do however agree on the direction of changes in PRCPTOT, suggesting that there will be an average of 5 fewer rain days each winter, a result which is statically significant mainly in the south. Rainfall indices during summer tend to display higher variability when compared to winter however these changes are not statistically significant. All models indicate that there will be areas where SDII increases markedly, by up to  $6 \text{ mm day}^{-1}$ , however models generally do not agree on the spatial distribution of these increases. Similarly each model shows patches of reduced intensity, by as much as  $-3 \text{ mm day}^{-1}$ . The ENS plots show those areas where models agree and it is apparent that results over large areas of the domain remain highly uncertain. W-CCS and W-ECH agree that the region's south coast will experience an increase in summer PRCPTOT however this is not supported by the W-CSI simulation, which shows a general decrease in summer

PRCPTOT. Overall, the simulated number of consecutive dry days (CDD) is expected to increase and the number of consecutive wet days (CWD) will decrease however these results are not found consistently across the region, nor are they statistically significant.

## 4 Discussion

### 4.1 Temperature changes

Significant increases in minimum and maximum temperatures found by the RCM are broadly consistent with SWWA temperature increases projected by the CMIP3 GCMs shown in Fig. 6 and found by others over this region (Suppiah et al. 2007). The RCM simulations illustrate a broader range of temperature change than GCMs in SWWA and their higher resolution allows for the development of finer spatial features in the distribution of warming. Suppiah et al. (2007) found a distinct north–south warming gradient while our results show that there is also an east–west

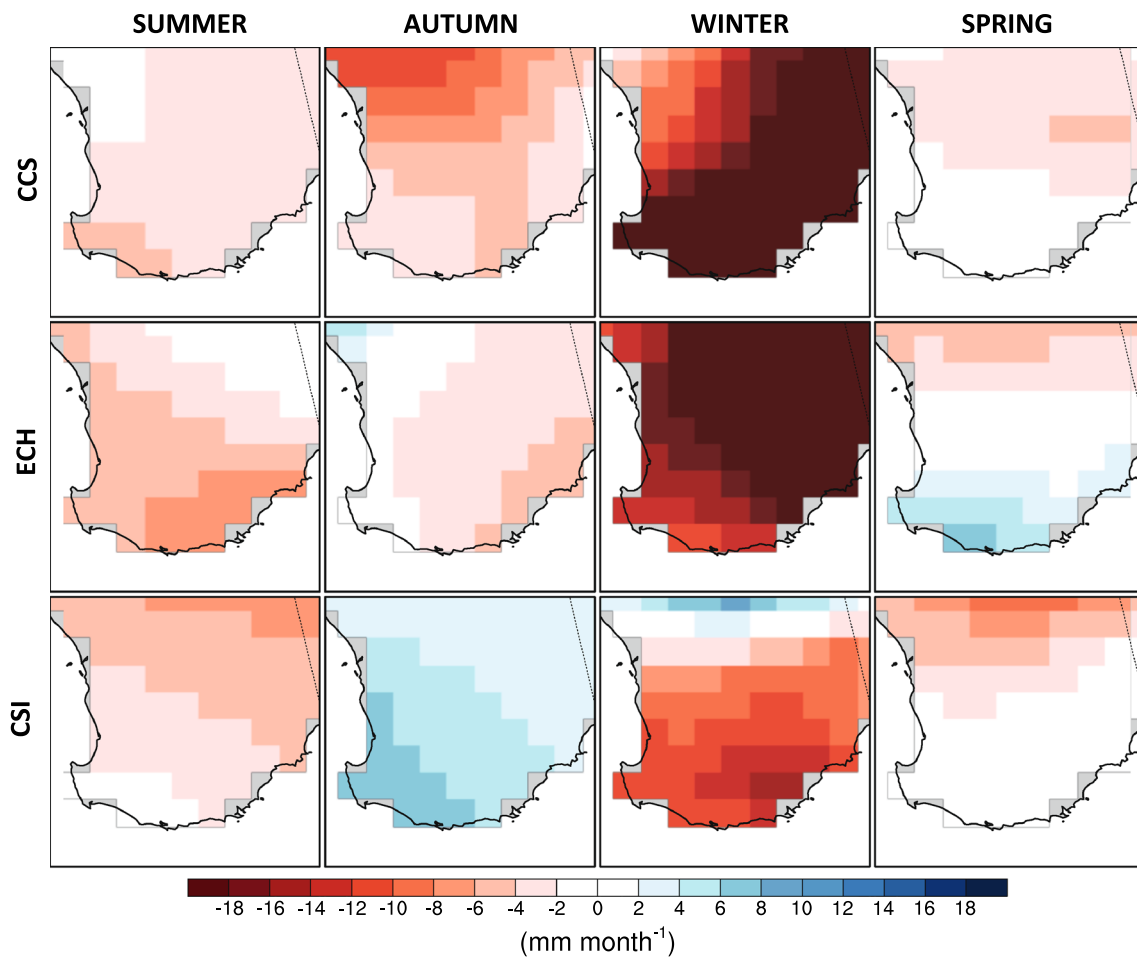


**Fig. 11** Mean seasonal rainfall differences (1970–1999 to 2030–2059) for the GCMs CCSM (CCS), CSIRO (CSI), ECHAM5 (ECH)

component to this gradient, particularly for summer and autumn maximum temperatures which show greater warming on the west coast of SWWA for W-CCS and W-ECH. Simulations showing greater warming along the coast differs from the findings of a number of GCM studies [for example Collins et al. (2013), Meehl et al. (2007)] because the highest rate of warming is most commonly projected to be inland; a response which is attributed to feedback from reduced relative humidity (Fasullo 2010). While this land sea thermal contrast is a major influence on temperature distribution at the resolution of the GCM, its influence at the scale of the RCM appears to be somewhat diminished as local effects are also resolved. The summer and autumn coastal soil moisture deficit seen in W-ECH and W-CCS (Fig. 9), caused by the simulated rainfall decline in these areas, results in increased sensible heat flux (Fig. 10). This results in the simulation of larger temperature increases on the coast compared to inland areas where there is a smaller decline in soil moisture. Our finding of a relationship between dry soils and sensible heat flux impacting daytime temperatures is supported by Fischer et al. (2007) and

Stéfanon et al. (2014) who found that soil moisture deficits contributed to higher maximum temperatures and hence heatwaves in western Europe. While GCMs also simulate soil moisture feedbacks, it is likely that the parameterisations and increased resolution of the RCM are enabling soil moisture to have a greater influence on temperature compared to the GCM. However, the ability of the WRF model to simulate soil moisture in SWWA has not been validated against observations and as such this model limitation needs to be considered when interpreting this finding.

Globally, GCMs tend to project a reduction in the future diurnal temperature range (DTR) (Collins et al. 2013). Reduced DTR is frequently attributed to an increase in cloud cover which inhibits outgoing longwave radiation and causes minimum temperatures to rise faster than maximum temperatures (Dai et al. 1999). Contrary to these findings, our results indicate that there is strong model agreement for increased DTR in SWWA. We explore possible attributions as to why this is the case and find that models simulate very little difference in mean seasonal cloud cover between the two climate periods. Models therefore suggest



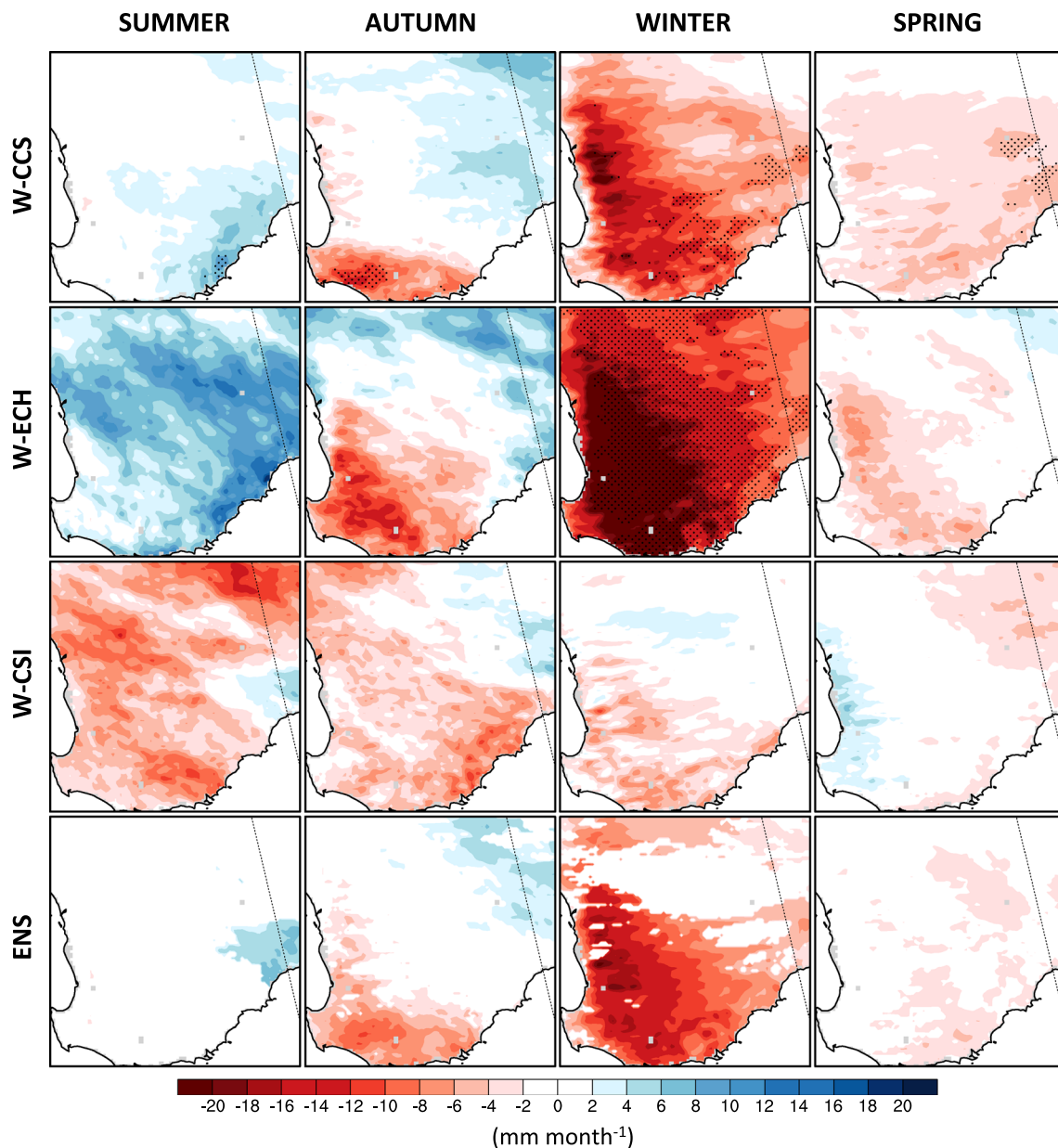


**Fig. 12** Seasonal mean rainfall differences between historical (1970–1999) and future (2030–2059) climate simulations. *Stippling* shows areas where there is a statistically significant difference at a 95 % confidence interval

that nighttime temperatures in SWWA may not experience amplified warming through increased cloud cover. However, this finding is uncertain because the performance of the model at replicating SWWA climatological cloud processes has not been evaluated as a part of this study. Summer soil moisture deficits have been associated with areas of enhanced daytime warming in SWWA and we now suggest that the soil moisture deficit, which is ubiquitous for all simulations in winter and spring, and the subsequent increase in daytime sensible heat flux is amplifying daytime warming in the model, leading to an increased DTR.

Standardised distributions of daily minimum and maximum temperature provide some evidence that there are changes in standard deviation between historical and future simulations (Figs. 4c, 5c). These are in line with the findings of Donat and Alexander (2012) who also found observed increases in nighttime temperature standard deviation in Western Australia. We do not examine possible attributions for increased nighttime temperature variability here, however we do note that previous studies examining Australian daily temperatures have suggested that distributions of temperature are compound in nature, comprising

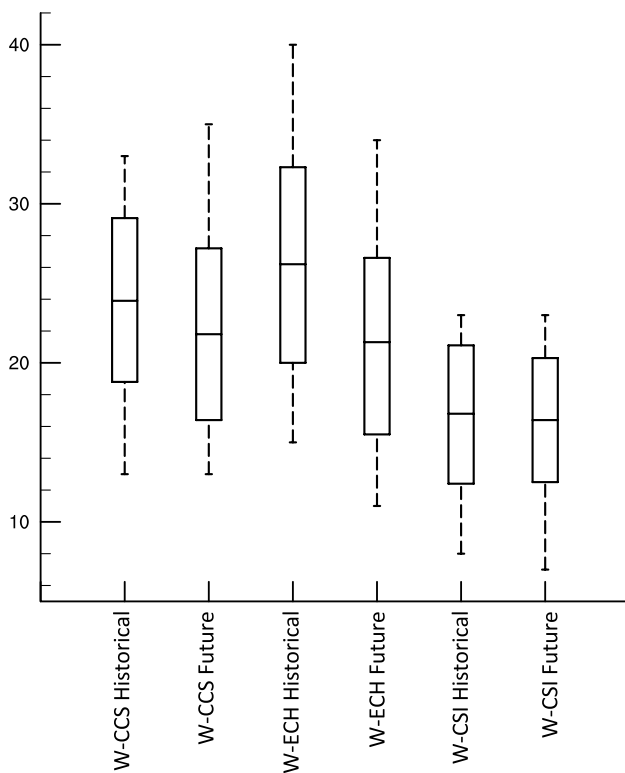


**Fig. 13** Boxplot showing the range of winter front days comparing historical (1970–1999) and future simulations. The *centre line* displays mean values, the box bounds one standard deviation from the mean and tails represent the range of values

of two or more distributions relating to specific air masses (Trewin 2001; Grace and Curran 1993). It is possible therefore, that increased variability is a result of unequal warming between the individual distributions comprising the compound distribution. Understanding the physical processes driving increased temperature variability will be the focus of future research.

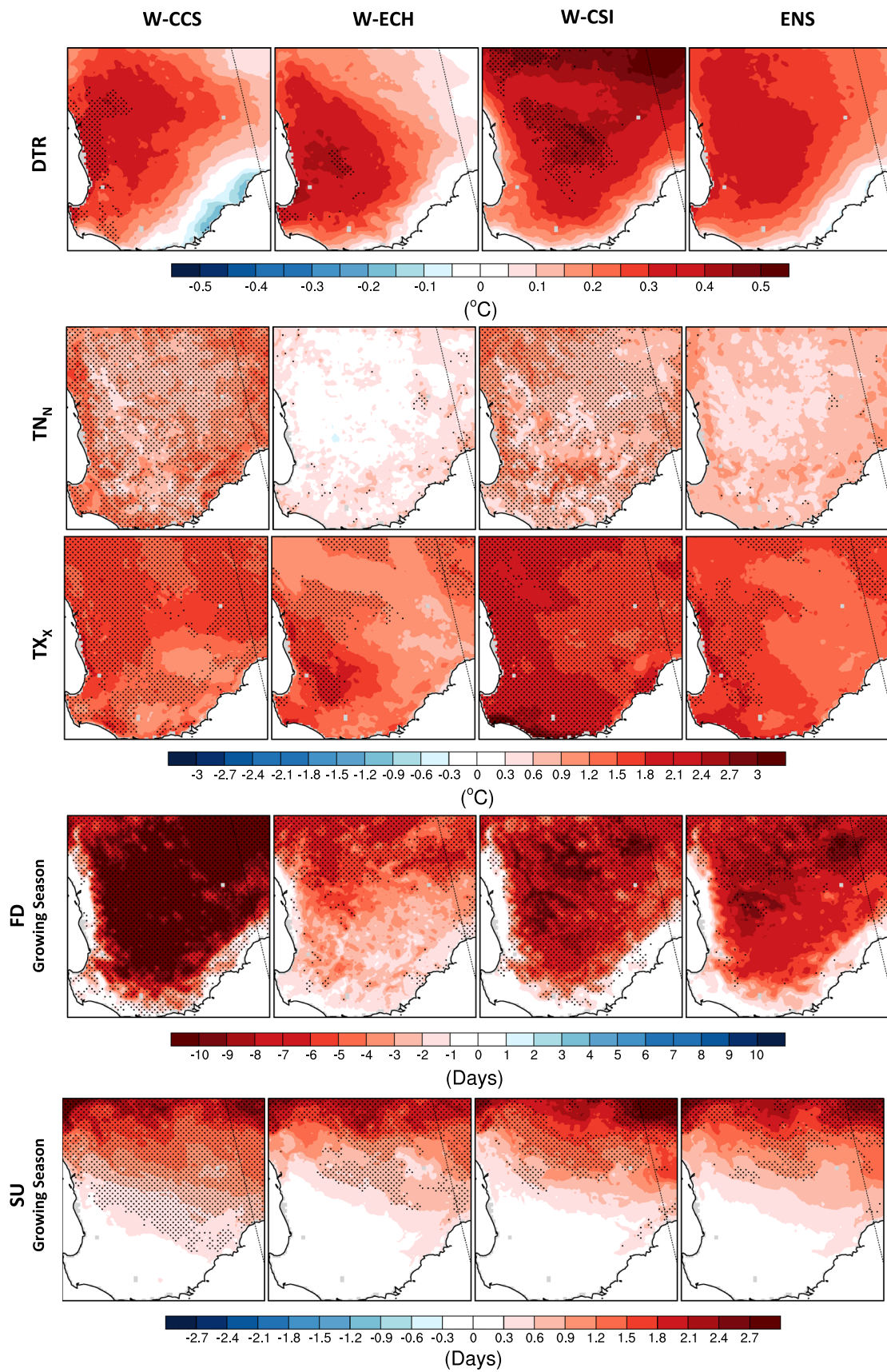
Statistically significant differences between the standardised distributions for W-CCS in areas where there is no change in standard deviation are apparent. This suggests that shifts in skewness and kurtosis may also contribute to differences between historical and future simulated temperature distributions. Perron and Sura (2013) examined a number of climate variables, including daily temperature distributions, and found that in addition to mean and standard deviation, the distribution of air temperature was also defined by skewness and kurtosis. Hence, our finding that skewness and kurtosis influence temperature distributions, is in line with the findings of Perron and Sura (2013). Positive changes to skewness indicate that the distribution is skewing further to the right, or hotter temperatures, while increases in kurtosis mean that the distribution is becoming more peaked, with more data in the middle of the distribution and less at the tails. Our simulations suggest that

**Fig. 14** Mean annual difference between historical (1970–1999) and future (2030–2059) for DTR,  $TX_X$  and  $TN_N$  temperature indices mean growing season difference is shown for the FD and SU indices. *Stippling* shows where the changes in the distribution of the indices is significant at the 95 % confidence level

the skewness and kurtosis of maximum temperatures may decrease in the future. Simulated minimum temperature kurtosis is also expected to decline however the direction of change in skewness is uncertain because models do not agree on the direction of the change. It is therefore apparent from our findings that changes in skewness and kurtosis exist between the historical and future climate simulations and more research is needed to understand both the statistical significance of these changes and their implications.

Notwithstanding, our simulation results indicate that the standard deviation of minimum temperatures is increasing. Nighttime temperature PDFs show an increased spread of temperatures and it is apparent that the  $TN_N$  index does not increase as much as mean nighttime temperatures in the simulation. Furthermore, standardised minimum temperature PDFs show a significant difference which is consistent across all simulations in the north west corner of SWWA and in patches on the southern coastline. Hence, these simulations suggest that, while average minimum temperatures are likely to increase, the likelihood of very cold nighttime temperatures may not necessarily decrease. Despite this finding, simulations do indicate that the incidence of frost, illustrated by the FD index in Fig. 14, in SWWA will decline significantly. Recent research on observed historical (1980–2011) frost trends in SWWA by Dittus et al. (2014) found that the number of frost days in some areas of SWWA is increasing, despite increases in average nighttime temperatures over the same period. The finding from our simulations of a future frost decline is in contrast to Dittus et al. (2014). One possible explanation for this contrast is that, by 2030, the simulated increase in mean nighttime temperature is large enough to offset the trend found by Dittus et al. (2014), outweighing the effect of increased minimum temperature variability on frost risk. Establishing this however requires further analysis as to whether WRF is able to capture the increasing trend in frost at these locations under current climate.

Only W-CSI and W-ECH PDFs show an increase in standard deviation for maximum temperatures, and increases in the  $TX_X$  index are fairly consistent with increases in mean summer daytime temperatures. Increased temperature variability has been found previously by Ylhaisi and Raisanen (2013) in the northern hemisphere mid-latitudes, however they found that the signal to noise ratio of increased variability outside of this region was generally low. These findings are consistent with our simulation results which do not suggest an increase in maximum



temperature variability. Furthermore, an analysis of temperature extremes by Kharin et al. (2007) found that changes in maximum temperature extremes generally followed mean changes in summer maximum temperatures and our simulations support this finding also. Notwithstanding, the significant increases in the  $TX_x$  and SU indices found in the simulations illustrate that mean temperature changes alone are sufficient to increase the likelihood of extreme temperature events. In particular, simulated increases in SU underscore the increased risk of heat stress in SWWA cereal crops in the future.

## 4.2 Rainfall changes

Compared to temperature results, there is far greater uncertainty as to the direction and magnitude of future precipitation changes in results from the RCM. This high degree of uncertainty is unsurprising because interannual rainfall variability in SWWA is much higher than temperature variability and GCMs generally demonstrate greater uncertainty with respect to precipitation (Alexander and Arblaster 2009). Notwithstanding, our simulation results show an overall decline in rainfall, particularly in winter which is the dominant rainfall season. Simulation results are generally consistent with findings from GCMs, shown in Fig. 11, and found by other GCM studies including the SWWA region (Suppiah et al. 2007). However, spatial patterns are apparent in the RCM results which are not found at the resolution of the GCM. For example, results from W-CCS and W-ECH highlight a differential rainfall decline in the vicinity of the Darling Scarp. In these simulations, rainfall on the western side of the Scarp is expected to experience a relatively small decline compared to the east of the Scarp.

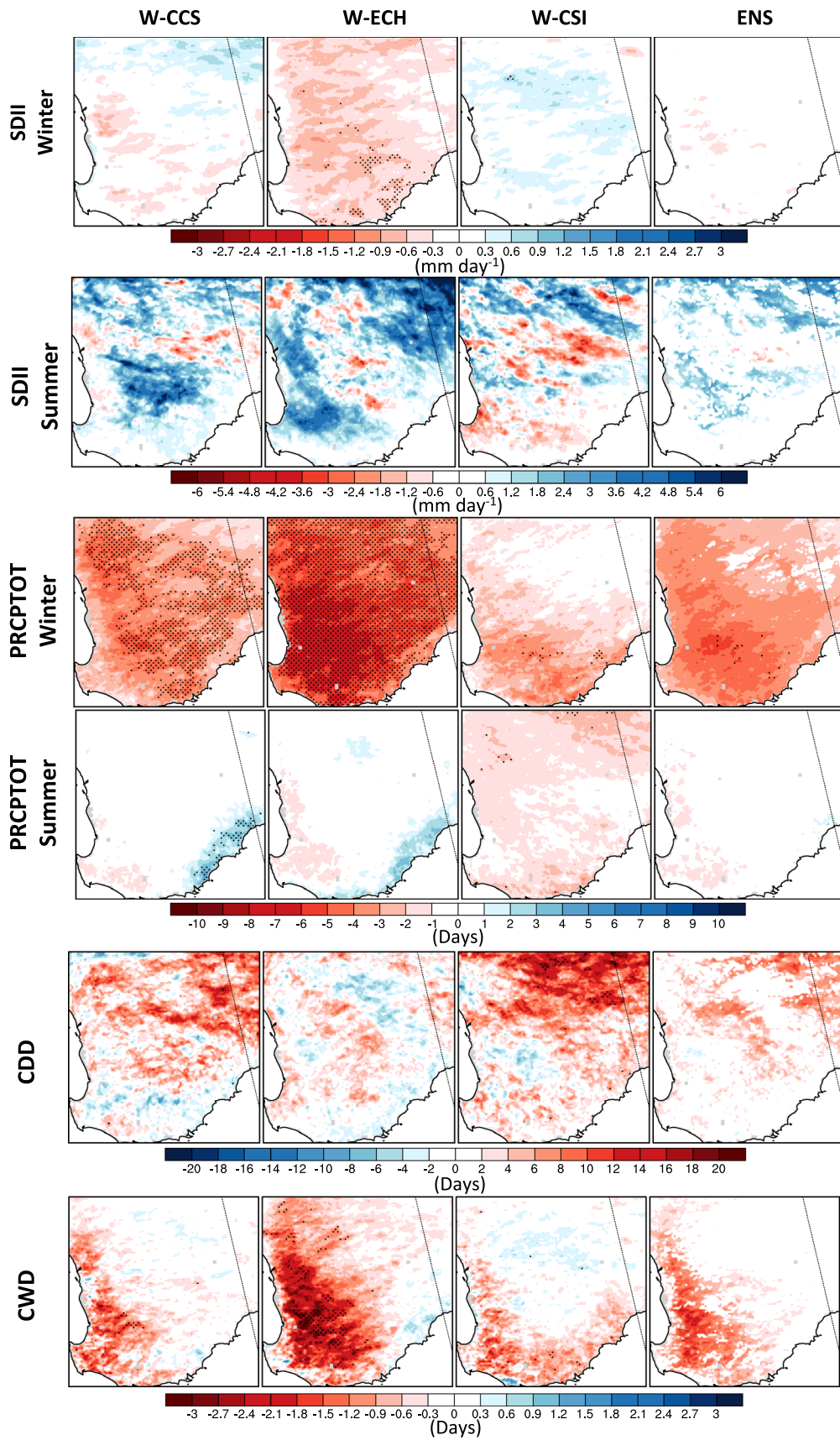
Historical winter rainfall decline in SWWA has been attributed to a poleward movement of the subtropical ridge, which diverts storm tracks to higher latitudes and results in fewer rain bearing cold fronts traversing the region. Seidel et al. (2008) found that this transition of the ridge could be attributed to the strengthening of the Hadley Cell and GCMs indicate that this strengthening will continue throughout the twenty-first century, reducing the baroclinic instability at the latitude of SWWA (Grainger et al. 2013). All of our simulations illustrate increased winter mean SLP to the south of Western Australia which reflects the projected ongoing poleward shift of the subtropical ridge. Smith et al. (2000) found that SLP was well correlated with winter rainfall in SWWA and could account for up to 60 % of rainfall variability. This relationship between SLP and rainfall is illustrated by the different winter rainfall responses between the three simulations; W-ECH has the largest winter SLP increase and the largest decline in winter rainfall. Conversely, W-CSI has the smallest

**Fig. 15** Mean summer and winter differences (1970–1999 to 2030–2059) for SDII and PRCPTOT. Mean annual differences are shown for CDD and CWD. *Stippling* shows areas where the difference is significant at a 95 % confidence interval

winter precipitation decline and shows very little change in SLP. Analysis of the number of simulated winter front days also suggests a decline in the number of cold fronts traversing the region, however these differences are generally small. Our finding that the simulated winter PRCPTOT is expected to decline by an average of approximately 5 days per season further supports the attribution of rainfall decline to fewer fronts traversing the region. However, it should be noted that fronts are not the only systems delivering winter rainfall to SWWA. Pook et al. (2012) demonstrated that cutoff lows are also responsible for rain in the region, particularly in the the autumn, and Risbey et al. (2013) showed that the rainfall from cutoff systems in the growing season has declined since the 1990s. While the rainfall contribution of cutoff lows is greatest in the autumn (Pook et al. 2012), these systems do contribute somewhat to winter rainfall. Because our study does not examine the occurrence of cutoff systems in the simulation, it is possible that winter changes in the frequency and/or magnitude of these systems events are impacting our findings on simulated frontal changes.

While there is strong evidence to support a poleward transition of the subtropical ridge and hence extra-tropical storms, there is little evidence to suggest an intensification or reduction in the strength of these systems (Bengtsson et al. 2009). It is therefore not surprising that our simulation results show little change in winter rainfall intensity. This result is also in line with the findings of Alexander and Arblaster (2009) who, in their analysis of CMIP3 GCMs, determined that SWWA SDII would remain fairly constant throughout the twenty-first century.

Changes to summer rainfall display less model agreement, and hence more uncertainty, than winter rainfall. Relative to the observed mean summer rainfall (Fig. 2), the magnitude of simulated changes are very large. For example, W-ECH projects that summer rainfall will as much as double in some areas. This increase can be attributed to an intensification of summer rainfall events as opposed to more frequent events. We refer to the fact that the simulated number of large scale summer rain events (Table 3) and summer PRCPTOT (Fig. 15) remain relatively constant as evidence to support this finding. Simulated changes to summer rainfall intensity are exceptionally large compared to our winter SDII and changes seen in other studies. For example, W-ECH shows summer SDII increases of up to  $6 \text{ mm day}^{-1}$  while other studies have reported annual changes to SDII of under  $0.001 \text{ mm day}^{-1}$  (Alexander and Arblaster 2009). The very large magnitude



of these intensity shifts can be attributed to the fact that simulated summer rainfall changes are relatively high and because there are so few summer rain days in the region. Consequently, a small number of very large rain events in the simulation can shift this index markedly, even over a 30 years climatology. SWWA summer rain events are caused by interactions with tropical disturbances in Australia's north west and recent work has established that the frequency and intensity of these disturbances has increased in the last two decades (O'Donnell et al. 2015). This trend is poorly represented in CMIP3 GCMs (Cai et al. 2011) and this uncertainty is a likely source of the lack of model agreement for summer rainfall changes seen in our results. Although our confidence in the simulated findings of summer rainfall change is low, the established impact of tropical cyclones on SWWA summer rainfall and the risk of serious consequences, including flash flooding and erosion of arable land, mean that a greater understanding of the processes driving summer rainfall in SWWA is needed.

Indices which measure the maximum length of wet (CWD) and dry (CDD) spells provide some indication of how rainfall patterns are likely to vary. Alexander and Arblaster (2009) found that by the end of the twenty-first century, SWWA can expect much longer dry spells. In our simulated results we find that, with the exception of the southern coast, CDD will increase by approximately 15 days a year and this result is significant over patches of the SWWA. Similarly, simulations show that the number of consecutive wet days will decline as fewer storms traverse the region in winter.

While our simulation ensemble has drawn from a number of GCMs to reduce uncertainty in our findings, the fact that we use only a single RCM configuration is a limitation of our experimental design because WRF has a known sensitivity to the choice of model physical parameterisations (Argueso et al. 2011). We note that other RCM studies [for example Evans et al. (2011)] use an ensemble of RCM configurations to reduce the uncertainty from using a single cohort of physical parameterisations. However, our research was limited by the computational resources required to undertake a larger ensemble using both multiple RCMs and GCMs. Our results are also constrained by limitations in our model domain configuration, which lead to high negative precipitation biases in the extreme south west corner of the region (Andrys et al. 2015b). As a consequence of these biases, future climate data from this small region should be interpreted with caution.

## 5 Conclusion

Projections of future climate change (2030–2059) for SWWA are analysed for a RCM ensemble using WRF with

lateral boundary conditions from three CMIP3 GCMs; CCSM3, CSIRO mk3.5 and ECHAM5. By dynamically downscaling GCM output, WRF provides climate data at a horizontal scale that allows for the resolution of local topography and the development of local effects, such as land atmosphere interactions, which have been found to have a strong impact on the climate of SWWA (Hirsch et al. 2014). We find that the RCM adds value to GCM output in SWWA by illustrating the importance of regional scale soil moisture feedback and its impact on enhanced daytime warming, and resolving differential rainfall changes in the vicinity of regional scale topography such as the Darling Scarp.

Our simulation results indicate that daytime temperatures will increase more than nighttime temperatures. This is attributed to a simulated decline in soil moisture which in turn increases sensible heat flux at the surface, hence amplifying daytime temperature increases and the DTR. Climate change is more commonly associated with a decline in DTR, caused by increased cloud cover enhancing the rate of nighttime warming, however we find no evidence for increased cloudiness in SWWA in these simulations. While the rate of nighttime warming is lower, simulations do provide evidence that the variability of minimum temperatures is increasing because the coldest nighttime temperatures are not increasing at the same rate as mean temperatures.

There is model consensus indicating a decline in winter rainfall and two of the simulations (W-ECH and W-CCS) show that this decline is statistically significant. However, there is little statistically significant change for all other seasons. W-ECH and W-CCS also show that the spatial distribution of winter rainfall decline is influenced by the Darling Scarp, because smaller rainfall reductions are expected on the western side of the Scarp than to the east. Declining winter rainfall is consistent with historical trends of rainfall in SWWA which is attributed to a southerly shift in storm tracks reducing the number of fronts passing over the region. The continuation of this southerly shift in storm tracks is indicated by the simulated increase in winter mean SLP in SWWA. We also find that the number of simulated winter front days and the number of winter precipitation days are expected to decrease. The lack of marked variation in winter SDII in the simulations indicates that the intensity of those winter storms which do bring rain to SWWA is not expected to change.

Summer precipitation in SWWA has been shown to be difficult to replicate (Andrys et al. 2015b; Kala et al. 2015) and this difficulty is reflected here as models vary widely in their projections. Unfortunately, this variation makes it difficult to draw any conclusions for summer rainfall. However, the summer SDII index does display some very large changes to precipitation intensity which, due to the potential risks posed by such considerable changes to

the hydrological regime, warrant further research to fully understand the mechanisms driving the projected changes.

Changes in temperature and precipitation are likely to impact cereal cropping in SWWA in the future. While agriculture is likely to benefit from a reduction in frost, this benefit may be offset by an ongoing decline in rainfall and the increased likelihood of heat stress which will be the greatest in the region's northeast.

We attribute the simulated spatial distribution of daytime warming to changes in soil moisture which in turn influences the partitioning of surface heat flux. Areas with soil moisture deficits show increased sensible heat flux and tend to display greater daytime temperature increases. Changes in soil moisture are predominantly caused by variations in rainfall and we have shown that simulated rainfall changes, with the exception of winter rainfall, are highly uncertain. Therefore, it follows that a degree of this uncertainty needs to be applied to our temperature findings also. Our research highlights the significance of interrelationships between climate variables and also the importance of land atmosphere interactions on climate in SWWA.

**Acknowledgments** This research was supported by an Australian Grains Research and Development Corporation (GRDC) Grant (MCV0013). Julia Andrys is supported by an Australian Postgraduate Award and a GRDC Top Up Scholarship. Jatin Kala was supported by the Australian Research Council Centre of Excellence for Climate Systems Science (CE110001028) for part of this work. The research group lead by Associate Professor Jason Evans at the University of New South Wales, Australia, provided the modified version of WRFv3.3 used in this study, and assisted in the pre-processing of the input data. Dr. Ruth Lorenz from the University of New South Wales provided the scripts to account for serial correlation in  $t$  tests. Computational modeling was supported by the Pawsey Supercomputing Centre with funding from the Australian Government and the Government of Western Australia. It was funded under the National Computational Merit Allocation Scheme and the Pawsey Partner Allocation Scheme. All of this support is gratefully acknowledged.

## References

- Alexander LV, Arblaster JM (2009) Assessing trends in observed and modelled climate extremes over Australia in relation to future projections. *Int J Climatol* 29:417–435. doi:[10.1002/joc.1730](https://doi.org/10.1002/joc.1730)
- Andrys J, Lyons TJ, Kala J (2015a) Evaluation of a WRF ensemble using GCM boundary conditions to quantify mean and extreme climate for the southwest of Western Australia (1970–1999). *Int J Climatol*. doi:[10.1002/joc.4641](https://doi.org/10.1002/joc.4641)
- Andrys J, Lyons TJ, Kala J (2015b) Multi-decadal evaluation of WRF downscaling capabilities over Western Australia in simulating rainfall and temperature extremes. *J Appl Meteorol Climatol* 54:370–394. doi:[10.1175/JAMC-D-14-0212.1](https://doi.org/10.1175/JAMC-D-14-0212.1)
- Argüeso D, Hidalgo-Mutildeno JM, Gacutemiz-Fortis SR, Esteban-Parra MJ, Dudhia J, Castro-Díez Y (2011) Evaluation of WRF parameterizations for climate studies over Southern Spain using a multi-step regionalization. *J Clim* 24:5633–5651. doi:[10.1175/JCLI-D-11-00073.1](https://doi.org/10.1175/JCLI-D-11-00073.1)
- Argüeso D, Hidalgo-Muñoz JM, Gámiz-Fortis SR, Esteban-Parra MJ, Castro-Díez Y (2012) Evaluation of WRF mean and extreme precipitation over Spain: present climate (1970–99). *J Clim* 25:4883–4897. doi:[10.1175/JCLI-D-11-00276.1](https://doi.org/10.1175/JCLI-D-11-00276.1)
- Asseng S, Foster I, Turner NC (2011) The impact of temperature variability on wheat yields. *Glob Change Biol* 17:997–1012. doi:[10.1111/j.1365-2486.2010.02262.x](https://doi.org/10.1111/j.1365-2486.2010.02262.x)
- Bates BC, Hope P, Ryan B, Smith I, Charles S (2008) Key findings from the Indian ocean climate initiative and their impact on policy development in Australia. *Clim Change* 89:339–354. doi:[10.1007/s10584-007-9390-9](https://doi.org/10.1007/s10584-007-9390-9)
- Bengtsson L, Hodges KI, Keenlyside N (2009) Will extratropical storms intensify in a warmer climate? *J Clim* 22:2276–2301. doi:[10.1175/2008JCLI2678.1](https://doi.org/10.1175/2008JCLI2678.1)
- Cai W, Cowan T, Sullivan A, Ribbe J, Shi G (2011) Are anthropogenic aerosols responsible for the northwest Australia summer rainfall increase? A CMIP3 perspective and implications. *J Clim* 24:2556–2564. doi:[10.1175/2010JCLI3832.1](https://doi.org/10.1175/2010JCLI3832.1)
- Chen F, Dudhia J (2001) Coupling an advanced land surface-hydrology model with the Penn State-NCAR MM5 modeling system. Part I: model implementation and sensitivity. *Mon Weather Rev* 129:569–585
- Collins M, Knutti R, Arblaster JM, Dufresne JL, Fichefet T, Friedlingstein P, Gao X, Gutowski WJ, Johns T, Krinner G (2013) Long-term climate change: projections, commitments and irreversibility. In: *In climate change 2013: the physical science basis. Contribution of working group I to the fifth assessment report of the intergovernmental panel on climate change*, Cambridge University Press, p 1054
- Collins WD, Rasch PJ, Boville BA, Hack JJ, McCaa JR, Williamson DL, Briegleb BP, Bitz CM, Lin SJ, Zhang M (2006) The formulation and atmospheric simulation of the Community Atmosphere Model version 3 (CAM3). *J Clim* 19:2144–2161. doi:[10.1175/JCLI3760.1](https://doi.org/10.1175/JCLI3760.1)
- Cover TM, Thomas JA (2012) *Elements of information theory*, 2nd edn. Wiley, Hoboken
- Dai A, Trenberth KE, Karl TR (1999) Effects of clouds, soil moisture, precipitation, and water vapor on diurnal temperature range. *J Clim* 12:2451–2473. doi:[10.1175/1520-0442\(1999\)012<2451:EOCSMP>2.0.CO;2](https://doi.org/10.1175/1520-0442(1999)012<2451:EOCSMP>2.0.CO;2)
- Dee DP, Uppala SM, Simmons aJ, Berrisford P, Poli P, Kobayashi S, Andrae U, Balmaseda Ma, Balsamo G, Bauer P, Bechtold P, Beljaars aCM, van de Berg L, Bidlot J, Bormann N, Delsol C, Dragani R, Fuentes M, Geer aJ, Haimberger L, Healy SB, Hersbach H, Hólm EV, Isaksen L, Kållberg P, Köhler M, Matricardi M, McNally aP, Monge-Sanz BM, Morcrette JJ, Park BK, Peubey C, de Rosnay P, Tavolato C, Thépaut JN, Vitart F (2011) The ERA-Interim reanalysis: configuration and performance of the data assimilation system. *Q J R Meteorol Soc* 137:553–597. doi:[10.1002/qj.828](https://doi.org/10.1002/qj.828)
- Dittus AJ, Karoly DJ, Lewis SC, Alexander LV (2014) An investigation of some unexpected frost day increases in southern Australia. *Aust Meteorol Oceanogr J* 64:261–271
- Donat MG, Alexander LV (2012) The shifting probability distribution of global daytime and night-time temperatures. *Geophys Res Lett* 39:L14707. doi:[10.1029/2012GL052459](https://doi.org/10.1029/2012GL052459)
- Donat MG, Leckebusch GC, Pinto JG, Ulbrich U (2010) European storminess and associated circulation weather types: future changes deduced from a multi-model ensemble of GCM simulations. *Clim Res* 42:27–43. doi:[10.3354/cr00853](https://doi.org/10.3354/cr00853)
- Dudhia J (1989) Numerical study of convection observed during the winter monsoon experiment using a mesoscale two-dimensional model. *J Atmos Sci* 46:3077–3107
- Evans B, Lyons T (2013) Bioclimatic Extremes drive forest mortality in southwest, Western Australia. *Climate* 1:28–52. doi:[10.3390/cli1020028](https://doi.org/10.3390/cli1020028)

- Evans JP, McCabe MF (2013) Effect of model resolution on a regional climate model simulation over southeast Australia. *Clim Res* 56:131–145. doi:[10.3354/cr01151](https://doi.org/10.3354/cr01151)
- Evans JP, Ekström M, Ji F (2011) Evaluating the performance of a WRF physics ensemble over South-East Australia. *Clim Dyn* 39(6):1241–1258. doi:[10.1007/s00382-011-1244-5](https://doi.org/10.1007/s00382-011-1244-5)
- Fasullo JT (2010) Robust land-ocean contrasts in energy and water cycle feedbacks. *J Clim* 23:4677–4693. doi:[10.1175/2010JCLI3451.1](https://doi.org/10.1175/2010JCLI3451.1)
- Feldmann H, Frueh B, Schaedler G, Panitz HJ, Keuler K, Jacob D, Lorenz P (2008) Evaluation of the precipitation for south-western Germany from high resolution simulations with regional climate models. *Meteorologische Zeitschrift* 17:455–465. doi:[10.1127/0941-2948/2008/0295](https://doi.org/10.1127/0941-2948/2008/0295)
- Fischer EM, Seneviratne SI, Vidale PL, Lüthi D, Schär C (2007) Soil moisture–atmosphere interactions during the 2003 European summer heat wave. *J Clim* 20:5081–5099. doi:[10.1175/JCLI4288.1](https://doi.org/10.1175/JCLI4288.1)
- Frederiksen JS, Frederiksen CS (2007) Interdecadal changes in southern hemisphere winter storm track modes. *Tellus Ser A Dyn Meteorol Oceanogr* 59:599–617. doi:[10.1111/j.1600-0870.2007.00264.x](https://doi.org/10.1111/j.1600-0870.2007.00264.x)
- Gao Y, Fu JS, Drake JB, Liu Y, Lamarque JF (2012) Projected changes of extreme weather events in the eastern United States based on a high resolution climate modeling system. *Environ Res Lett.* doi:[10.1088/1748-9326/7/4/044025](https://doi.org/10.1088/1748-9326/7/4/044025)
- Gentili J (1971) *Climates of Australia and New Zealand*. Elsevier Pub. Co., Amsterdam
- Gordon HB, Rotstayn LD, McGregor JL, Dix MR, Kowalczyk EA, O'Farrell SP, Waterman LJ, Hirst AC, Wilson SG, Collier MA (2002) *The CSIRO Mk3 climate system model*, vol 130. CSIRO Atmospheric Research
- Grace W, Curran E (1993) A binomial model of frequency distributions of daily maximum temperature. *Aust Met Mag* 42:151–161
- Grainger S, Frederiksen CS, Zheng X (2013) Modes of interannual variability of Southern Hemisphere atmospheric circulation in CMP3 models: assessment and projections. *Clim Dyn* 41:479–500. doi:[10.1007/s00382-012-1659-7](https://doi.org/10.1007/s00382-012-1659-7)
- Grell GA, Emeis S, Stockwell WR, Schoenemeyer T, Forkel R, Michalakes J, Knoche R, Seidl W (2000) Application of a multiscale, coupled MM5/chemistry model to the complex terrain of the VOTALP valley campaign. *Atmos Environ* 34:1435–1453
- Hirsch AL, Kala J, Pitman AJ, Carouge C, Evans JP, Haverd V, Mocko D (2014) Impact of land surface initialization approach on subseasonal forecast skill: a regional analysis in the Southern Hemisphere. *J Hydrometeorol* 15:300–319. doi:[10.1175/JHM-D-13-05.1](https://doi.org/10.1175/JHM-D-13-05.1)
- Hong SY, Dudhia J, Chen SH (2004) A revised approach to ice microphysical processes for the bulk parameterization of clouds and precipitation. *Mon Weather Rev* 132:103–120. doi:[10.1175/1520-0493\(2004\)132<0103:ARATIM>2.0.CO;2](https://doi.org/10.1175/1520-0493(2004)132<0103:ARATIM>2.0.CO;2)
- Hope P, Keay K, Pook M, Catto J, Simmonds I, Mills G, McIntosh P, Risbey J, Berry G (2014) A comparison of automated methods of front recognition for climate studies: a case study in southwest Western Australia. *Mon Weather Rev* 142:343–363. doi:[10.1175/MWR-D-12-00252.1](https://doi.org/10.1175/MWR-D-12-00252.1)
- Hughes L (2003) Climate change and Australia: trends, projections and impacts. *Austral Ecol* 28:423–443. doi:[10.1046/j.1442-9993.2003.01300.x](https://doi.org/10.1046/j.1442-9993.2003.01300.x)
- Jones DA, Wang W, Fawcett R (2009) High-quality spatial climate data-sets for Australia. *Aust Meteorol Oceanogr J* 58:233–248
- Kain JS (2004) The Kain-Fritsch convective parameterization: an update. *J Appl Meteorol* 43:170–181
- Kala J, Lyons TJ, Foster IJ, Nair US (2009) Validation of a simple steady-state forecast of minimum nocturnal temperatures. *J Appl Meteorol Climatol* 48:624–633. doi:[10.1175/2008JAMC1956.1](https://doi.org/10.1175/2008JAMC1956.1)
- Kala J, Andrys J, Lyons TJ, Foster IJ, Evans B (2015) Sensitivity of WRF to driving data and physics options on a seasonal time-scale for the southwest of Western Australia. *Clim Dyn* 44:633–659. doi:[10.1007/s00382-014-2160-2](https://doi.org/10.1007/s00382-014-2160-2)
- Kharin VV, Zwiers FW, Zhang X, Hegerl GC (2007) Changes in temperature and precipitation extremes in the IPCC ensemble of global coupled model simulations. *J Clim* 20:1419–1444. doi:[10.1175/JCLI4066.1](https://doi.org/10.1175/JCLI4066.1)
- Leibensperger EM, Mickley LJ, Jacob DJ, Chen WT, Seinfeld JH, Nenes A, Adams PJ, Streets DG, Kumar N, Rind D (2012) Climatic effects of 1950–2050 changes in US anthropogenic aerosols-part I: aerosol trends and radiative forcing. *Atmos Chem Phys* 12:3333–3348. doi:[10.5194/acp-12-3333-2012](https://doi.org/10.5194/acp-12-3333-2012)
- Malcolm JR, Liu C, Neilson RP, Hansen L, Hannah LEE (2006) Global warming and extinctions of endemic species from biodiversity hotspots. *Conserv Biol* 20:538–548. doi:[10.1111/j.1523-1739.2006.00364.x](https://doi.org/10.1111/j.1523-1739.2006.00364.x)
- Meehl GA, Stocker TF, Collins WD, Friedlingstein P, Gaye AT, Gregory JM, Kitoh A, Knutti R, Murphy JM, Noda A (2007) Global climate projections. In: 2007: the physical science basis. Contribution of working group I to the fourth assessment report of the intergovernmental panel on climate change, vol 283, chap 10. Cambridge University Press, Cambridge, pp 747–846
- Mishra V, Dominguez F, Lettenmaier DP (2012) Urban precipitation extremes: how reliable are regional climate models? *Geophys Res Lett* 39(L03):407. doi:[10.1029/2011GL050658](https://doi.org/10.1029/2011GL050658)
- Mlawer EJ, Taubman SJ, Brown PD, Iacono MJ, Clough SA (1997) Radiative transfer for inhomogeneous atmospheres: RRTM, a validated correlated-k model for the longwave. *J Geophys Res* 102(D):16,663–16,682. doi:[10.1029/97JD00237](https://doi.org/10.1029/97JD00237)
- Nakićenović N, Alcamo J, Davis G, De Vries B, Fenhann J, Gaffin S, Gregory K, Grübler A, Jung T, Kram T (2000) IPCC special report on emissions scenarios (SRES), working group III, Intergovernmental Panel on Climate Change (IPCC). Cambridge University Press, Cambridge
- Naveau P, Guillou A, Rietsch T (2014) A non-parametric entropy-based approach to detect changes in climate extremes. *J R Stat Soc* 76:861–884. doi:[10.1111/rssb.12058](https://doi.org/10.1111/rssb.12058)
- O'Donnell AJ, Cook ER, Palmer JG, Turney CSM, Page GFM, Grierson PF (2015) Tree rings show recent high summer-autumn precipitation in Northwest Australia is unprecedented within the last two centuries. *PloS One*. doi:[10.1371/journal.pone.0128533](https://doi.org/10.1371/journal.pone.0128533)
- Perkins SE, Pitman AJ, Holbrook NJ, McAneney J (2007) Evaluation of the AR4 climate models' simulated daily maximum temperature, minimum temperature, and precipitation over Australia using probability density functions. *J Clim* 20:4356–4376. doi:[10.1175/JCLI4253.1](https://doi.org/10.1175/JCLI4253.1)
- Perron M, Sura P (2013) Climatology of non-Gaussian atmospheric statistics. *J Clim* 26:1063–1083. doi:[10.1175/JCLI-D-11-00504.1](https://doi.org/10.1175/JCLI-D-11-00504.1)
- Persson G, Barring L, Kjellström E (2007) Climate indices for vulnerability assessments. 111, SMHI
- Pielke RA, Wilby RL (2012) Regional climate downscaling: what's the point? *Eos Trans Am Geophys Union* 93:52–53. doi:[10.1029/2012EO050008](https://doi.org/10.1029/2012EO050008)
- Pitts RO, Lyons TJ (1990) Airflow over a two-dimensional escarpment. II: hydrostatic flow. *Q J R Meteorol Soc* 116:363–378. doi:[10.1002/qj.49711649207](https://doi.org/10.1002/qj.49711649207)
- Pook MJ, Risbey JS, McIntosh PC (2012) The synoptic climatology of cool-season rainfall in the central wheatbelt of Western Australia. *Mon Weather Rev* 140(1):28–43
- Risbey JS, Pook MJ, McIntosh PC (2013) Spatial trends in synoptic rainfall in southern Australia. *Geophys Res Lett* 40(14):3781–3785. doi:[10.1002/grl.50739](https://doi.org/10.1002/grl.50739)



- Roeckner E (2003) The atmospheric general circulation model ECHAM 5. Part I: model description, rep. 349, Max Planck Inst. for Meteorol., Hamburg
- Salathé EP, Leung LR, Qian Y, Zhang Y (2010) Regional climate model projections for the state of Washington. *Clim Change* 102:51–75. doi:10.1007/s10584-010-9849-y
- Seidel DJ, Fu Q, Randel WJ, Reichler TJ (2008) Widening of the tropical belt in a changing climate. *Nat Geosci* 1:21–24. doi:10.1038/ngeo.2007.38
- Shukla J, DelSole T, Fennessy M, Kinter J, Paolino D (2006) Climate model fidelity and projections of climate change. *Geophys Res Lett* 33(L07):702. doi:10.1029/2005GL025579
- Smith IN, McIntosh P, Ansell TJ, McInnes K (2000) Southwest Western Australian winter rainfall and its association with Indian Ocean climate variability. *Int J Climatol* 1930:1913–1930. doi:10.1002/1097-0088(200012)20:15<1913:AID-JOC594>3.0.CO;2-J
- Song R, Gao X, Zhang H, Moise A (2008) 20 km resolution regional climate model experiments over Australia: experimental design and simulations of current climate. *Aust Meteorol Mag* 57:175–193
- Stéfanon M, Drobinski P, D’Andrea F, Lebeaupin-Brossier C, Bastin S (2014) Soil moisture–temperature feedbacks at meso-scale during summer heat waves over Western Europe. *Clim Dyn* 42:1309–1324. doi:10.1007/s00382-013-1794-9
- Suppiah R, Hennessy KJ, Whetton PH, McInnes K, Macadam I, Bathols J, Ricketts J, Page CM (2007) Australian climate change projections derived from simulations performed for the IPCC 4th assessment report. *Aust Meteorol Mag* 56:131–152
- Taylor KE, Stouffer RJ, Meehl Ga (2012) An overview of CMIP5 and the experiment design. *Bull Am Meteorol Soc* 93:485–498. doi:10.1175/BAMS-D-11-00094.1
- Tippett MK, Kleeman R, Tang Y (2004) Measuring the potential utility of seasonal climate predictions. *Geophys Res Lett* 31:1–4. doi:10.1029/2004GL021575
- Trewin BC (2001) Extreme temperature events in Australia. Submitted in total fulfilment of the requirements of the degree of Doctor of Philosophy, October 2001. School of Earth Sciences, The University of Melbourne
- Turner NC, Asseng S (2005) Productivity, sustainability, and rainfall-use efficiency in Australian rainfed Mediterranean agricultural systems. *Crop Pasture Sci* 56:1123–1136. doi:10.1071/AR05076
- Varnas D (2014) Western Australian grains industry. <https://www.agric.wa.gov.au/grains-research-development/western-australian-grains-industry>
- Webb LB, Watterson I, Bhend J, Whetton PH, Barlow EWR (2013) Global climate analogues for winegrowing regions in future periods: projections of temperature and precipitation. *Aust J Grape Wine Res* 19:331–341. doi:10.1111/ajgw.12045
- Wehner M, Smith R, Bala G, Duffy P (2010) The effect of horizontal resolution on simulation of very extreme US precipitation events in a global atmosphere model. *Clim Dyn* 34:241–247. doi:10.1007/s00382-009-0656-y
- Wright PB (1974) Seasonal rainfall in Southwestern Australia and the general circulation. *Mon Weather Rev* 102:219–232
- Xue Y, Janjic Z, Dudhia J, Vasic R, De Sales F (2014) A review on regional dynamical downscaling in intraseasonal to seasonal simulation/prediction and major factors that affect downscaling ability. *Atmos Res* 147–148:68–85. doi:10.1016/j.atmosres.2014.05.001
- Ylhäisi JS, Raisanen J (2013) Twenty-first century changes in daily temperature variability in CMIP3 climate models. *Int J Climatol* 1428:1414–1428. doi:10.1002/joc.3773
- Zheng B, Chenu K, Fernanda Dreccer M, Chapman SC (2012) Breeding for the future: what are the potential impacts of future frost and heat events on sowing and flowering time requirements for Australian bread wheat (*Triticum aestivum*) varieties? *Glob Change Biol* 18:2899–2914. doi:10.1111/j.1365-2486.2012.02724.x
- Zwiers FW, von Storch H (1995) Taking serial correlation into account in tests of the mean. *J Clim* 8:336–351. doi:10.1175/1520-0442(1995)008<0336:TSCIAI>2.0.CO;2